Structure of the Ponga Unit: evidence for secondary oroclinal buckling in the foreland fold and thrust belt of the Variscan orogen, Cantabrian orocline, northern Spain

by

Kassandra Del Greco
B.Sc., McGill University, 2012

A Thesis Submitted in Partial Fulfillment
of the Requirements for the Degree of

MASTER OF SCIENCE

in the School of Earth and Ocean Sciences

Supervisory Committee

Structure of the Ponga Unit: evidence for secondary oroclinal buckling in the foreland fold and thrust belt of the Variscan orogen, Cantabrian orocline, northern Spain

by

Kassandra Del Greco
B.Sc., McGill University, 2012

Supervisory Committee

Dr. Stephen T. Johnston (School of Earth and Ocean Sciences)
Supervisor

Dr. Kristin Morell (School of Earth and Ocean Sciences)
Departmental Member

Abstract

Supervisory Committee
Dr. Stephen T. Johnston (School of Earth and Ocean Sciences)
Supervisor
Dr. Kristin Morell
Departmental Member

The origin of the Cantabrian orocline of the Variscan orogen in NW Iberia remains a topic of debate. We present a structural study of the Ponga Unit, a Cambrian to Carboniferous tectonostratigraphic package within the Variscan foreland fold and thrust belt that lies within the core region of the Cantabrian orocline. Our primary goal is to determine if the structure of the Ponga Unit is attributable to secondary orocline formation or if west-plunging regional folds in the area reflect lateral ramps in underlying Variscan thrust sheets.

Our mapping and structural analysis within the Ponga Unit focuses on the Laviana, Rioseco and Campo de Caso thrust sheets, and associated bounding thrusts. More than 800 structural orientation measurements were collected across the study area during a four-week field campaign. These data, coupled with data compiled from regional geological maps, allow for analysis of the crustal structure. West-plunging folds of the Laviana, Rioseco and Campo de Caso thrust sheets form km-scale anticline-syncline pairs, producing a complex fold interference pattern that is characteristic of the Ponga Unit. Our analysis shows that: 1) the geometry of the west-plunging folds is inconsistent with a lateral-ramp related interpretation; 2) the map pattern resembles a mushroom fold interference pattern that is the result of two deformation phases including secondary, orocline-related N-S shortening immediately after the cessation of E-W Variscan shortening; and 3) paleomagnetic data, notably a ‘B’ remanence magnetism, in the Ponga Unit likely overlaps in time with the cessation of Variscan deformation and records post-Variscan deformation associated with the onset of oroclinal buckling. Our results indicate that early N-S trending folds, which resulted from Variscan orogenesis, were refolded by a N-S oriented compressive stress that is attributable to the secondary buckling of the Cantabrian orocline.

Table of Contents

List of Tables

List of Figures

Acknowledgments

I would like to first thank my supervisor Stephen Johnston for his mentorship, insightfulness and patience over the past few years. I was consistently encouraged by him to think critically and challenged to work independently as an academic. Acknowledgements to Gabi Gutiérrez-Alonso and Javier Fernández Lozano for their initial guidance on the ground in Spain as well as for the roles they played as I started this project two years ago. I would like to extend my appreciation to my committee members, and to all those that I had the pleasure to learn and work with during my tenure at UVic. These individual include Kristen Morell, Duncan Johannessen, David Nelles, Theron Finley, and Lucinda Leonard among others.

A very special thanks is owed to Jessica Shaw for not only being a mentor and inspiration, but for her tireless help and advice on my project and her most important role as my best friend in Victoria. I would also like to thank my friends and fellow graduate students Duncan MacKay, Tiegan Hobbs, Bennit Mueller, Siobhan McGoddrick, Travis Dawson, Mitchell Wolf, Alicia Lew and Sarah Jackson for welcoming me, elevating me and making Victoria feel like home.

I will forever be indebted to my absolutely incredible parents, Anne Journeaux and Angelo Del Greco, for supporting and encouraging me in my decision to complete a Master's degree, as well as in every decision I have ever made, and to my brother Zach Del Greco for always reminding me that life has to be fun.

Funding for this project was provided by an NSERC Discovery Grant awarded to my supervisor Stephen T. Johnston, and a University of Victoria Graduate Award.

Chapter 1. Introduction

1.1 Motivation

The motivation of this study is to further understand the mechanisms of orocline formation. Carey first coined the term 'orocline' in 1955, defining it as a thrust or orogenic belt that has been curved about a vertical axis of rotation. There are two, end-member, models for orocline formation (Johnston et al., 2013) (Figure 1 - 1). A progressive orocline forms progressively and simultaneously during orogenesis (Figure 1 - 1a). Progressive oroclines are thin-skinned, restricted to a thrust sheet or thrust belt and are the result of an orogen-perpendicular principal compressive stress (Johnston et al., 2013). A secondary, or 'Carey', orocline is one that is formed after initial orogenesis has occurred (Figure 1 – 1b). Secondary oroclines are orogen scale, thick-skinned map-view curves. Secondary oroclines form as a result of a change in principal compressive stress from an orogen-perpendicular one during orogenesis to a post-orogenic orogen-parallel one (Johnston et al., 2013).

The Cantabrian orocline is the northern member of the coupled Iberian oroclines of the Variscan orogen (Figure 1 - 2). Due to its geologic exposure and ease of access, the Cantabrian orocline is the most studied orocline in the world. There is significant disagreement regarding the mechanism of formation of the Cantabrian orocline. Primary models, in which the orocline is interpreted to have formed as a result of progressive deformation during Variscan orogenesis (Brun and Burg, 1982; Pérez-Estaún et al., 1988; Ribeiro et al., 1995, 2007; Martínez Catalán, 2011a), and secondary models, in which the orocline is inferred to have formed as a result of a post-orogenic switch in the orientation of the principal compressive stress to an orogen-parallel orientation (Parés et al., 1994;

Van der Voo et al., 1997; Weil et al., 2000, 2001; Merino-Tomé et al., 2009; Weil et al., 2010; Pastor-Galán et al., 2011; Weil et al., 2013a) have been proposed. This study aims to evaluate the structure at the core of the Cantabrian orocline in order to further assess how the Cantabrian orocline formed. Understanding the formation of the Cantabrian orocline is: 1) crucial to understanding the processes responsible for supercontinent formation; 2) specifically important in understanding Pangean paleogeography and tectonics leading up to the end Permian mass extinction; and 3) central to determining the processes responsible for orocline formation.

1.2 Structure of dissertation

This thesis examines map-scale, west-plunging folds located in the Ponga Unit, a tectonostratigraphic package consisting of a thrust-imbricated stratigraphic sequence within the Variscan foreland fold and thrust belt that lies in the core of the Cantabrian orocline of Iberia. The Ponga Unit contains several thrust sheets that are up to 4 km thick and is composed of Cambrian, Ordovician and Carboniferous strata (Julivert, 1971). The map-scale folds of the Ponga Unit have classically been interpreted to be the result of progressive deformation during orogenesis (Pérez-Estaún et al., 1988; Alvarez-Marrón, 1995).

Chapter 2, "Interference folding and orocline implications: a structural study of the Ponga Unit, Cantabrian orocline, northern Spain", presents the results of a detailed structural analysis of the Ponga Unit and discusses the formation of kilometer scale, west-plunging, folds. We compare two end-member models for the formation of the Ponga Unit folds, one that relates folding to progressive deformation during Variscan orogenesis and one that relates folding to secondary deformation during oroclinal buckling after

Variscan orogenesis. Chapter 2 was co-authored by Dr. Stephen T. Johnston, Dr. Gabriel Gutiérrez-Alonso, Dr. Jessica Shaw and Dr. Javier Fernández Lonzano. Johnston and Gutiérrez-Alonso helped define the project and assisted with mapping. Shaw, who completed a Ph.D. on the Iberian oroclines, helped place our findings within a regional tectonic framework. Fernández-Lozano assisted with mapping and with the digital database development. As first author, I led the mapping program, compiled available structural data, undertook the structural analyses of the map area and wrote the paper.

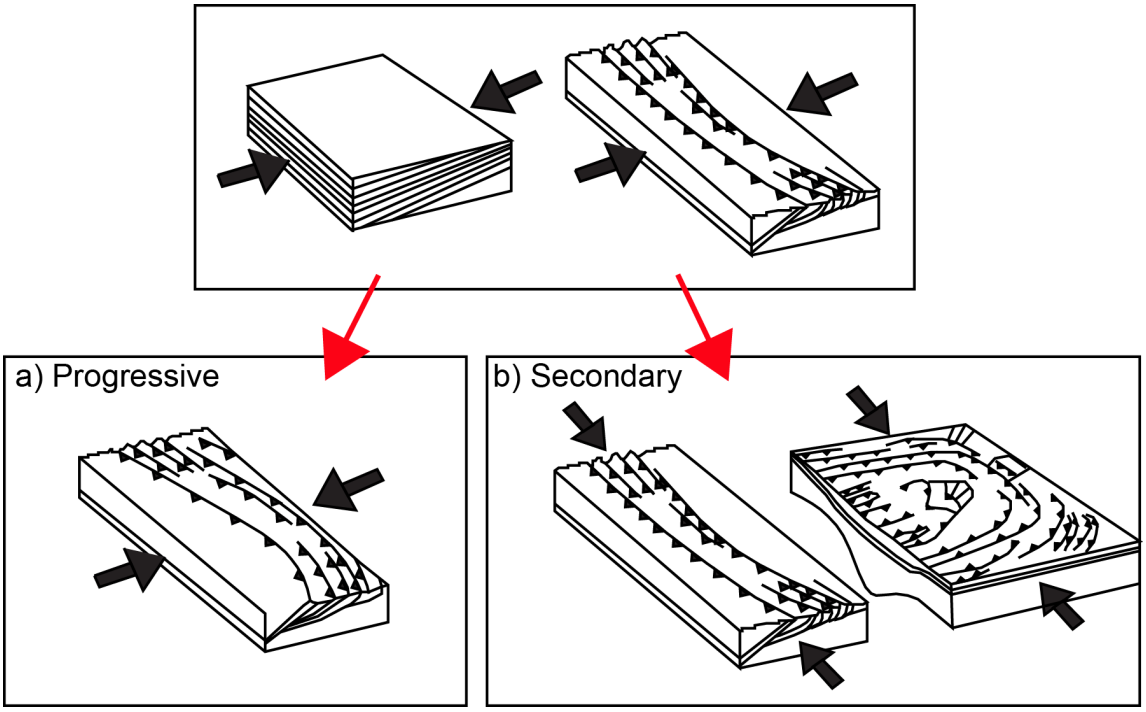

Figure 1 - 1 Series of block diagrams depicting the formation of (a) a progressive orocline in response to orogen-perpendicular stress during orogenesis and (b) formation of a secondary orocline after a change in stress from an orogen-perpendicular one to an orogen-parallel one. Modified from Johnston et al. (2013).

1.3 Location of the study area

The Ponga Unit is located in the Principality of Asturias, an autonomous community located in northwestern Spain. The field area spanned ~20 km by ~20 km, and was located 50 km SE of Oviedo, Spain, and 100 km North of León, Spain. Mountains that range in elevation from 1200 m to 2000 m define the study area. The topography is controlled by, and is a reflection of, the distribution of the Ordovician Barrios (Armorican) Formation, a hard, robust quartzite.

1.4 Methods of investigation

Fieldwork for this study was carried out from June 8th to July 11th, 2014. The small towns of Felechosa, Caleao and Rioseco, Spain, were the basis for all field-mapping operations. Mapping traverses were completed by the author and Theron Finley (undergraduate field assistant) on foot. Additional mapping support was provided by Dr. Gabriel Gutiérrez-Alonso (University of Salamanca), Dr. Javier Fernández Lozano (University of Salamanca) and Dr. Stephen Johnston (Supervisor, University of Victoria) during their visits to the field area.

Mapping was completed using a station-based system where lithological and structural data were collected and assigned to a GPS waypoint location with a station ID. All GPS data is accurate to ~5 meters. Planar and linear structural data were collected for each station using a compass. All data were input into ArcGIS. Maps of the region by Alvarez-Marrón et al. (1990), Caride et al. (1973), Heredia and Rodriguez Fernández, (1989) and Velando et al. (1973) were utilized to guide our mapping, and were modified in light of our findings. All structural analyses were conducted using Stereonet® (Allmendinger et al., 2011).

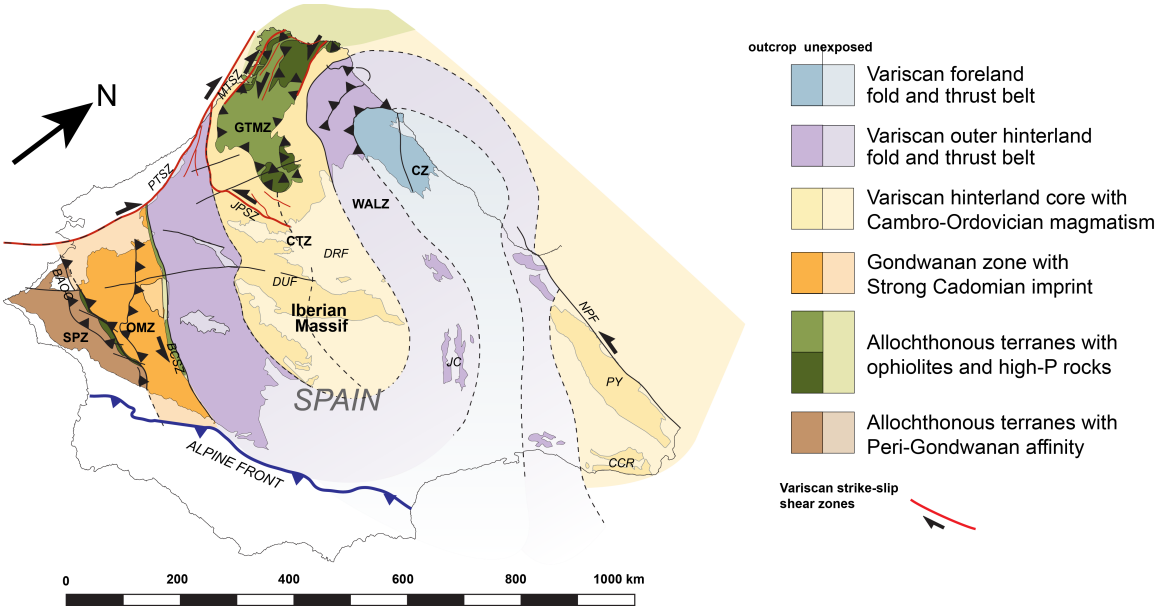

Figure 1 - 2 Tectonostratigraphic zones across the Western European Variscan belt. Coupled Cantabrian orocline and Central Iberian oroclines indicated by dashed lines. BAOC—Beja-Acebuches ophiolitic complex; BCSZ—Badajoz-Cordóba shear zone: CCR—Catalonian Coast Ranges; CZ—Cantabrian Zone; CIZ—Central Iberian Zone; DRF—Domain of Recumbent folds; DUF—Domain of Upright folds;GTMZ—Galicia-Trás-os-Montes Zone; IC—Iberian Cordillera; JPSZ—Juzbado-Penalvashear zone; MTSZ—Malpica-Tui suture zone; OMZ—Ossa Morena Zone; PTSZ—Porto-Tomar shear zone; PY—Pyrenees; SPZ—South Portuguese zone; WALZ—West Asturian-Leonese zone. Modified from Shaw et al. (2012).

1.5 Previous work

The Ponga Unit was first described, by Julivert (1962, 1971), as a subunit of the Cantabrian Zone (Figure 1 - 2). It consists of several thrust sheets in which maximum horizontal displacement is several tens of kilometers. Julivert and Marcos (1973) and Julivert and Arboleya (1984) published studies on the structural geology of the

Cantabrian Zone. Julivert described the map-view folds of the Ponga Unit and compared them to a Type 2 fold interference pattern as per Ramsay (1962).

Existing geologic maps of the Ponga Unit were created by Alvarez-Marrón et al. (1990), Caride et al. (1973), Heredia and Rodriguez Fernández, (1989) and Velando et al. (1973). Alvarez-Marrón and Pérez-Estaún undertook extensive mapping of the Ponga Unit and have published multiple papers (Pérez-Estaún et al., 1988; Alvarez Marrón, 1989; Alvarez-Marrón, 1995) describing their results. They interpreted the west-plunging folds of the Ponga Unit as fault-bend folds attributable to lateral ramps in the underlying thrust faults.

Hirt et al. (1992), Stewart (1995) and Weil (2006) have undertaken paleomagnetic investigations of the area. Weil (2006) used data from previous paleomagnetic studies in combination with his collected data to interpret the folds of the Ponga Unit to be, in part, as a result of lateral-ramp related interference during thrust sheet emplacement.

Chapter 2. Interference folding and orocline implications: A structural study of the Ponga Unit, Cantabrian orocline, northern Spain[1]

2.1 Abstract

The origin of the Cantabrian orocline of the Variscan orogen in NW Iberia remains a topic of debate. We present a structural study of the Ponga Unit, a Cambrian to Carboniferous tectonostratigraphic package within the West European Variscan Belt foreland fold-and-thrust belt that lies within the core region of the orocline. Our primary goal is to determine if west-plunging folds of the fold and thrust belt are attributable to formation of the Cantabrian orocline or if they reflect lateral ramps in the underlying Variscan thrust faults.

The major lithological units of the Ponga are the rheologically competent Lower Ordovician Barrios quartzite, and the less competent, Carboniferous Barcaliente limestone and Beleño shale and sandstone formation. Our mapping and structural analysis within the Ponga Unit focused on the Laviana, Rioseco and Campo de Caso thrust sheets, and associated bounding thrusts. Over 800 structural orientation measurements were collected across the study area. These data, coupled with data compiled from regional geological maps, allow for analysis of the crustal structure. West-plunging folds of the Laviana, Rioseco and Campo de Caso thrust sheets form km-scale anticline-syncline pairs, producing a complex fold interference pattern that is

[1] This chapter is in published as: Del Greco, K., Johnston, S.T., Gutiérrez-Alonso, G., Shaw, J., and Fernández Lozano, J., 2016, Interference folding and orocline implications: a structural study of the Ponga Unit, Cantabrian orocline, northern Spain: Special Issue Article, Lithosphere.

characteristic of the Ponga Unit. Our analysis shows that: 1) the geometry of the west-plunging folds is inconsistent with a lateral ramp model; 2) the map pattern defines a mushroom-type fold-interference pattern, indicating two distinct deformational events characterized by principal compressive stresses oriented at a high angle (perpendicular) to one another; and 3) paleomagnetic data from the study area are consistent with the secondary model of orocline formation and indicate that there was a geologically instantaneous window of time between the end of Variscan orogenesis and the onset of oroclinal buckling. Our results indicate that early N-S trending folds, which resulted from Variscan orogenesis, were refolded during a post-Variscan orogen-parallel compression event attributable to formation of the Cantabrian orocline.

2.2 Introduction

The origin of bends, as observed in map-view, of mountain systems and orogenic belts is debated. End-member 'progressive' and 'secondary' models make testable predictions about the timing and processes involved in the development of such bends. In 'Progressive models', curvature is thin-skinned, develops 'progressively' during orogenesis due to local vertical-axis rotations, and is driven by the same stress field responsible for orogenesis. Indentation by continental promontories is probably the most common 'Progressive' model applied to explain curved continental collisional orogens. Examples include the Appalachian Kinston orocline (Marshak and Tabor, 1989) and the Cordilleran Wyoming Salient (Weil et al., 2010). In contrast, 'Secondary' models explain bends as thick-skinned, vertical-axis buckles that accommodate strike-parallel shortening of a pre-existing orogen. 'Secondary' bends, which are referred to as oroclines, necessarily post-date orogenesis, and require a principal compressive stress

orthogonal to the initial ‘orogenic’ stress. Examples include the Alaskan oroclines that characterize the Cordillera of western North America (Johnston, 2001) and the Carpathian - Balkan oroclines of the Alpine orogen (Shaw and Johnston, 2012).

The collisional Variscan orogen of northern Iberia is characterized by a convex to the west hairpin bend that is commonly referred to as the Cantabrian orocline (Suess, 1909) (Figure 2 - 1). Progressive and secondary models have been proposed to explain Cantabrian orocline formation. Progressive explanations include the involvement of a continental promontory (Lefort, 1979; Murphy et al., 2016) or corner (Brun and Burg, 1982); non-cylindrical deformation (Pérez-Estaún et al., 1988; Martínez-Catalán, 1990); and syn-orogenic strike-slip shearing (Martínez Catalán, 2011; Aerden, 2004). Secondary models include bending of a linear Variscan orogen in response to buckling of the continental core of Pangea about a pole of rotation at the western end of the Tethyan embayment (Gutiérrez-Alonso et al., 2008); an unexplained 90-degree rotation of the stress field (Ries and Shackleton, 1976; Van der Voo et al., 1997; Weil et al., 2001; Aerden, 2004); a clockwise rotation of Gondwana which produced a 90-degree rotation of the stress field (Pastor-Galán et al., 2015); and buckling of a ribbon continent (Shaw and Johnston, in review).

The Cantabrian orocline is cored by the Variscan east-verging, foreland fold and thrust belt within which a Precambrian to Carboniferous stratigraphic sequence is imbricated and folded. Thrust faults strike south and verge east within the Cantabrian orocline core. Folds include sub-horizontal fault-bend folds that are inferred to reflect a stair-step, flat-ramp-flat fault geometry and a second set of folds that plunge west and are characterized by steep to vertical, E-W striking axial planes. The second set of folds is

responsible for imparting a complex, sinuous map-pattern on the region. These folds potentially provide us with the means for testing the Progressive and Secondary models of the Cantabrian orocline. Interpretation of the E-W trending folds as reflecting lateral ramps within the underlying thrust faults (Pérez-Estaún et al., 1988; Alvarez-Marrón, 1995) explains all the faults and folds as products of E-W convergence, consistent with progressive models of Cantabrian orocline development. Alternatively, interpretation of the E-W trending folds as post-Variscan structures developed during strike-parallel, N-S shortening of the Variscan orogeny (e.g. Weil et al., 2013a and Johnston et al., 2013), requires a principal compressive stress orthogonal to the Variscan stress field, consistent with models of the Cantabrian orocline as a secondary orocline.

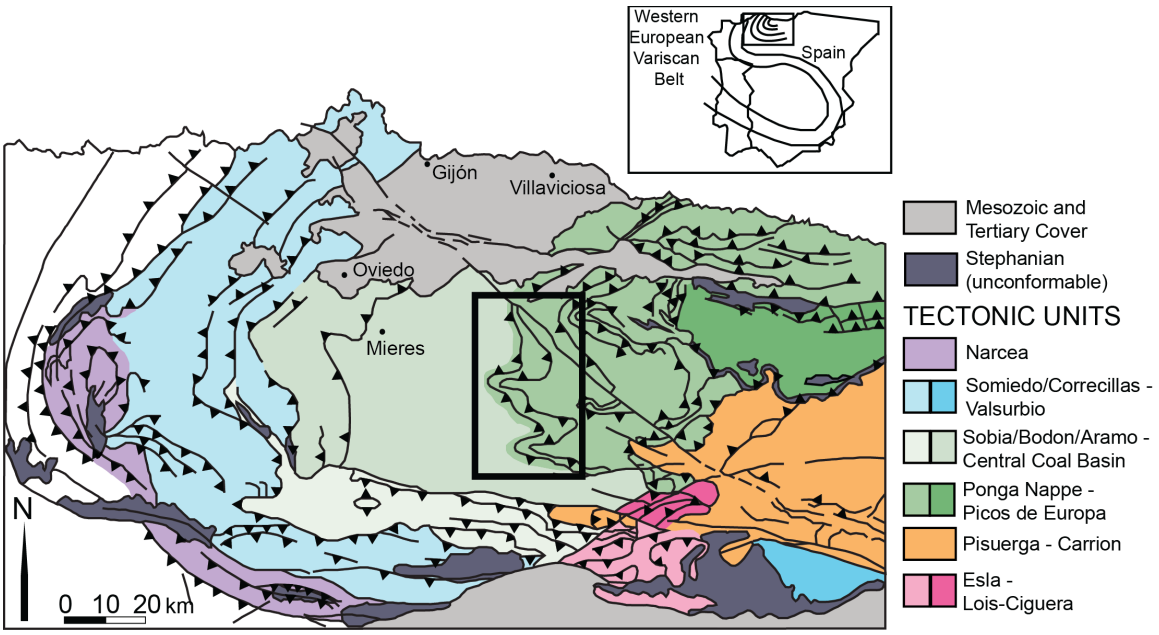

Figure 2 - 1 Figure showing the location of the Ponga Unit within the Cantabrian orocline of Northern Iberia. Modified from Weil, 2006.

In order to distinguish between these contrasting explanations, we undertook a detailed structural study of the Ponga Unit, a thrust nappe within the fold and thrust belt in the core of the Cantabrian orocline. We review the geological setting of the Variscan orogen, and summarize the stratigraphy and regional structure of the Ponga Unit, prior to presenting a structural analysis of our study area. Our data allow us to construct detailed downplunge projections that we have used to constrain the geometry of the thrust sheets that characterize the Ponga Unit, and the geometry of the E-W trending folds of the thrust sheets. Aerden (2004) interpreted the folds of the Ponga Unit to be representative of progressive changes in principal compressive stress during the Variscan orogeny. However, due to lack of observed evidence of progressive superpositions of folding during the Variscan orogeny, the high amplitude and, short, regular wavelength (~11 km) of the E-W trending folds requires significant N-S shortening of the entire fold-and-thrust belt. Therefore, we propose that these folds formed during a post-Variscan event characterized by a principal compressive stress orthogonal to the previous Variscan stress field.

2.3 Geological setting

The Devonian - Carboniferous Variscan orogen of western Europe is interpreted as a product of the Pangea-forming continental collision of Gondwana and Laurussia upon closure of an intervening 'Rheic' ocean (e.g. Nance et al., 2010). The Variscan foreland fold and thrust belt is referred to as the Cantabrian zone in Iberia. The zone is characterized by a Paleozoic sedimentary succession including Cambrian to Ordovician passive margin strata, and a younger Carboniferous foreland-basin sequence. The passive margin sedimentary succession consists of carbonates and siliciclastics that are

interpreted to have been deposited along the north margin of Gondwana (Shaw et al., 2014) during opening of the Rheic Ocean. The Rheic Ocean is inferred to have opened between a more northerly series of 'peri-Gondwana' terranes that drifted north from Gondwana, starting in the Cambrian (Nance et al., 2010), and autochthonous Gondwana to the south. The Carboniferous sequence consists of syntectonic carbonates and siliciclastic sedimentary rocks that were deposited into the Variscan foreland basin (Julivert, 1971). The fold and thrust belt is characterized by thrust faults that cut up section toward the foreland and verge to the east (Julivert, 1971). As in classic fold and thrust belts, the sedimentary sequences of the foreland-basin strata thin toward the foreland and the décollement surface dips toward the hinterland (Pérez-Estaún et al., 1994, 1995; Gallastegui et al., 1997). Synkinematic remagnetization and structural data restrict deformation in the fold and thrust belt to between 320 and 310 Ma (Parés et al., 1994; Van der Voo et al., 1997; Weil et al., 2000, 2001, 2010, 2012; Weil, 2006; Pérez-Estaún et al., 1988).

The Cantabrian Zone is divisible into six tectonic units that are defined by stratigraphy and structure (Figure 2 - 1): (1) the Narcea; (2) the Somiedo/Correcillas; (3) the Central Coal Basin; (4) the Ponga Nappe/Ponga Unit; (5) Picos de Europa; and (6) Pisuerga - Carrion units. The Ponga Unit lies east of the Central Coal Basin and west of the Pisuerga-Carrión and Picos de Europa units. It contains several thrust sheets; most notably the Laviana, Rioseco and Campo de Caso thrust sheets, and is characterized by a thin-skinned deformation style. These thrust sheets are up to 4 km thick, and carry Cambrian, Ordovician and Carboniferous strata (Julivert, 1971).

2.4 Stratigraphy and regional structure of the Ponga Unit

From oldest to youngest, the main Cambro-Ordovician formations that characterize the Ponga Unit include the Láncara, Oville and Barrios formations (Figure 2 - 2). The Middle Cambrian Láncara Formation is a 50 - 150m thick carbonate sequence (Julivert, 1971). The overlying Upper Cambrian to Lower Tremadocian Oville Formation consists of shales and sandstones (Julivert, 1971) which are in turn overlain by quartzite of the Barrios Formation (hereafter referred to as the Barrios quartzite). The Barrios quartzite is locally up to 750 m thick in places and consists of pure white quartzite, with thin volcanic ash layers, beds of phyllitic siltstones, and minor shale layers (Shaw et al., 2012). The Barrios quartzite is an important stratigraphic and structural marker horizon within the study area. It is correlative with the Armorican quartzite - an extensive quartzite unit that can be traced across West Africa, Armorica, Western Europe, and as far east as Serbia (Gutiérrez-Alonso et al., 2007). In the study area, the Barrios quartzite consistently underlies the topographically highest terrain, and forms near vertical faces that give the mountains of the Ponga Unit their dramatic appearance.

A thin Upper Ordovician black shale unit ("Pizarras del Sueve") and conglomerate and sandstone of the early Carboniferous Ermita Formation (~50 m thick) are locally present above the Barrios quartzite. These two units are only preserved in the northern syncline of the Laviana thrust sheet (Gutiérrez-Marco et al., 2002 and references therein). There are no Devonian strata preserved within the study area.

The main Carboniferous foreland basin units are, in ascending order, the Alba, Barcaliente, Beleño/Fresnedo, and Redonda/Escalada Formations, and the Fito/Lena Group (Figure 2 - 2). The Upper Famennian/lower Tournaisian Alba Formation

(Colmenero et al., 2002) is a ~20 - 40 m thick nodular, iron bearing, red limestone unit. Above the Alba formation is the 200 - 500 m thick black, azoic, Serpukhovian Barcaliente Formation limestone (also known as the Caliza de Montaña or Mountain Limestone Formation).

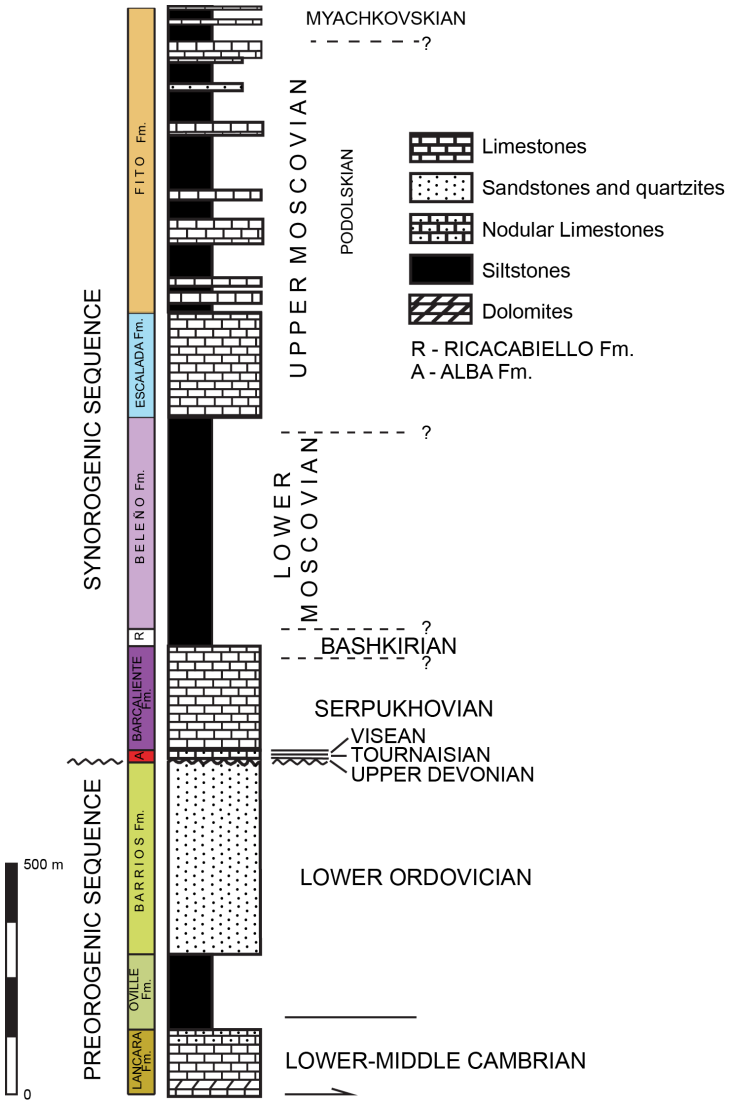

Figure 2 - 2 Stratigraphic column of the Ponga Unit. Modified from Alvarrez-Marrón and Pérez-Estaún (1988).

The overlying Moscovian Beleño (named Fresnedo in the Laviana thrust sheet) Formation is commonly over 500 m thick, consists of shales and channelized turbiditic sandstones, with thin, interbedded, limestones, rooted horizons and coal seams near the top of the unit (Colmenero et al., 2002). Above the Beleño Formation is the only cliff-forming Carboniferous unit, the 200 – 300 m thick, Moscovian, grey to white, micritic and skeletal limestone. It is named the Redonda or Escalada Formation (in the Laviana and Campo de Caso thrust sheets, respectively) (Colmenero et al., 2002).

The uppermost unit, the Moscovian Fito or Lena Group (in the Laviana and Campo de Caso thrust sheets, respectively) consists of over 1000 m of shales with interbedded limestones, sandstones and coal seams. The Beleño Formation and Fito/Lena Group are marine basin fill sequences that thin landward toward the east (Bahamonde, 1990; Bahamonde and Colmenero, 1993).

Our focus is on the Laviana, Rioseco and Campo de Caso thrust sheets (Figure 2 - 3). It is the surface traces of these thrust sheets that form a series of four folds (kilometer-scale), two of which are anticlines and two of which are synclines. The vector of motion of the thrust sheets during emplacement, as defined by cut-off lines, fold axes, minor shear bands and the orientation of map-scale fault-bend folds, is 090 (Alvarez Marrón, 1989; Alvarez-Marrón, 1995). Therefore, the vector of thrust sheet emplacement lies in the E-W striking axial planes of km-scale regional folds that deform the thrust sheets. The thrust sheets are characterized by a stair-step (flat–ramp–flat) geometry (Pérez-Estaún et al., 1988) and are locally characterized by recumbent. Locally recumbent folds are characterized by fold axes that parallel the strike of the thrust faults and are interpreted as thrust-propagation structures. Alvarez-Marón and Pérez Estaún (1988) concluded,

through palinspastic restoration of E-W oriented balanced cross-sections, that the minimum amount of accumulated transport by these three thrust sheets was 62 km. The Laviana, Rioseco and Campo de Caso thrusts root to the west into a décollement located at the base of the Lower-Middle Cambrian Lancara Formation. The regional folds affecting the thrust sheets include the Beleño and Tarna synclines and the Rio Monasterio and San Isidro anticlines (Figure 3). Siliciclastic shale and sandstone units, such as the Fito Formation and the Beleño Formation, are characterized by a steeply-dipping, irregular, scaly cleavage that is commonly steep to vertical, strikes parallel to adjacent thrust faults, and is assumed to have formed during Variscan thrusting.

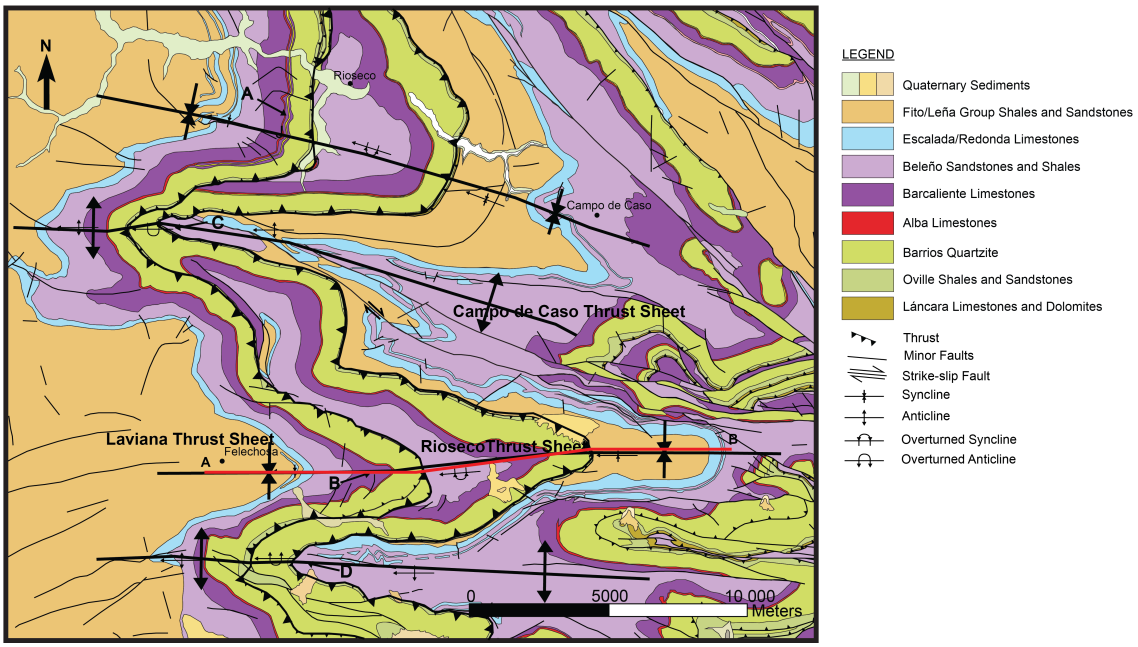

Figure 2 - 3 Geological map of the Ponga Unit in the study area showing the Laviana, Rioseco and Campo de Caso thrust sheets, Beleño (A) and Tarna (B) synclines, Rio Monasterio (C) and San Isidro (D) anticlines. Cross-section A-B location is displayed in red. Modified fromAlvarez-Marrón et al., 1990, Caride et al., 1973, Heredia et al., 1989 and Velando et al., 1973.

2.5 Data

The majority of our data were collected across the Tarna syncline and the Rio Monasterio anticline.

2.5.1 Bedding and Minor Folds

Over 800 structural orientation measurements on bedding planes and minor fold axes were collected across the 400 km^2 study area. In addition, we compiled existing data from regional geological maps. The majority of bedding measurements were collected from the ridge-forming Barrios quartzite, outcrops of which are commonly well bedded. Bedding data were also collected from the Escalada/Redonda limestone, the Barcaliente limestone, the Beleño Formation and the Fito/Lena Group. The incompetent and readily deformable shales and sandstones of the Beleño Formation rarely preserve primary bedding structures, however this unit was host to many (~42%, n=18) of the measurable minor, cm to dm scale, fold axes. The minor folds resulted from folding of the steeply dipping scaly cleavage. The Fito/Lena Group, which is similarly incompetent, hosted ~33% (n=15) of the minor folds of the scaly cleavage. Neither the massive limestone units nor the Barrios Quartzite exhibited evidence of pervasive deformation, which we attribute to their rheological competency.

To facilitate our structural analysis, we defined six structural domains. Domain boundaries include major thrust faults, an E-W striking line across the inflection point between the Rio Monasterio anticline and the Tarna syncline and a late strike-slip fault that cuts across the map area (Figure 2 - 4). As indicated by the map-pattern and by the great circle distribution of the poles to bedding in each of the six domains, the thrust sheets are folded. The folds plunge westwards and the magnitude of the plunge decreases

regularly from west to east. Cylindrical best-fit analyses for bedding data in the six domains are displayed in Figure 2 - 4 and Table 2 - 1.

The plunge of west-plunging fold axes does not vary more than 1º within thrust sheets. A cylindrical best fit analysis for bedding data show: the Laviana thrust sheet gives a fold axis plunging 60º towards 266º; the Rioseco thrust sheet gives a fold axis plunging 41º towards 267º; and the Campo de Caso thrust sheet gives a fold axis plunging 33º toward 264º. A west to east decrease in the fold plunge is consistent with the western thrust sheets having being steepened by displacement over ramps in the younger, underlying thrust sheets to the east. A stereonet plot of poles to bedding for the entire study area yields a regional fold axis plunging 48º towards 265º.

Analysis of the minor fold axes, measured in the scaly cleavage, yielded a high concentration (31%) of hinge-lines measured on minor folds that plunge over 60° (Figure 2 - 5). A comparison of the orientation minor fold axes with regional folds shows that steeply-plunging fold axes are pervasive in the study area. The variation in fold axes in the scaly cleavage is influenced by three factors: (1) Variscan folding; (2) vertical-axis rotation during oroclinal buckling; and (3) flow of less competent units towards the noses of regional folds. Regional structural studies of the Cantabrian orocline (Shaw et al., 2016) show that such map-scale steeply-plunging cross-folds are restricted to the core of the orocline.

Table 2 - 1 Trend and Plunge of major folds in small domains

Domain	1	2	3	4	5	6
Plunge (º)	62	43	34	62	42	34
Trend (º)	273	270	263	258	258	264

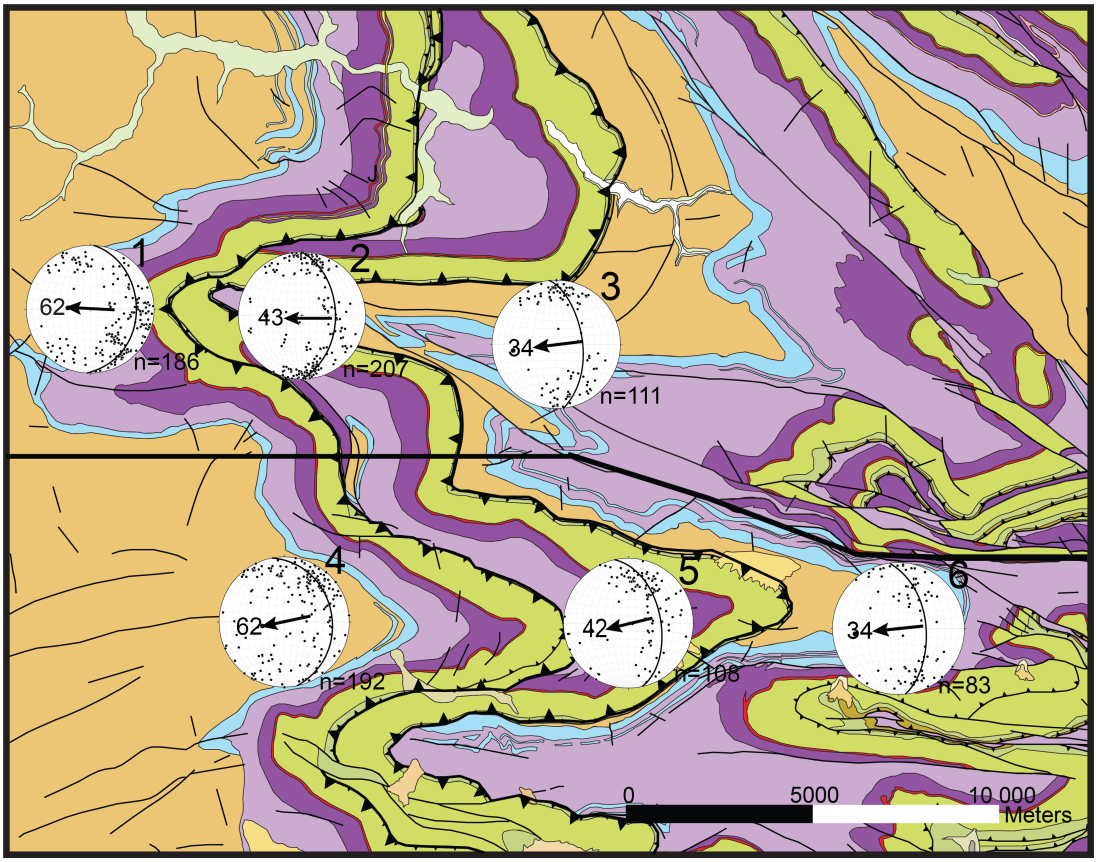

Figure 2 - 4 Stereonet plots for six domains defined according to thrust sheets and an inflection point and fault line between the Rio Monasterio anticline and the Tarna syncline. Fold axes defined by cylindrical best fit of bedding data are displayed for each domain: 1) 62 → 273; 2) 43 → 270; 3) 34 → 263 4) 62 → 258; 5) 42 → 258; 6) 34 → 264. Number of data points analyzed in each domain is indicated by value of *n*. Plunge of fold axes decreases from West to East. See Figure 2 - 3 for legend. Modified fromAlvarez-Marrón et al., 1990, Caride et al., 1973, Heredia et al., 1989 and Velando et al., 1973

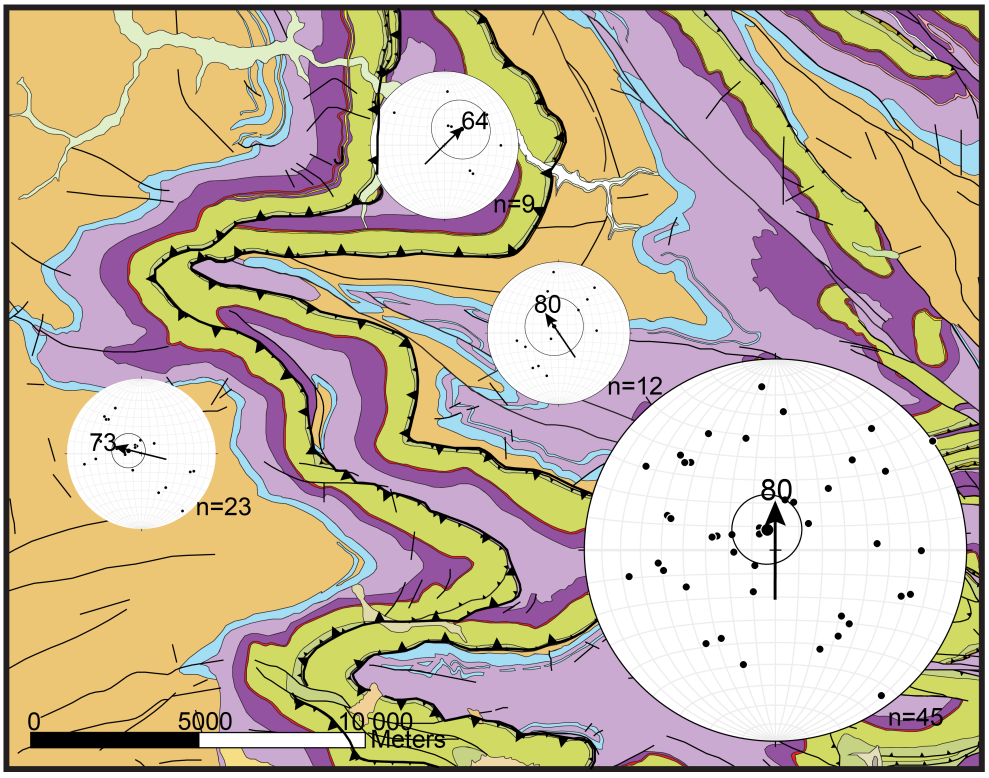

Figure 2 - 5 Map showing minor fold axis stereonet analysis for individual thrust sheets (small stereonets) and for the entire map area (large stereonet). Mean vectors are displayed on stereonets. Number of data analyzed per stereonet is indicated by *n*. Small circles on stereonets indicate 2nd standard deviation. Mean vector of all minor fold axes indicates a plunge steeper than 60º. See Figure 2 - 3 for legend. Modified fromAlvarez-Marrón et al., 1990, Caride et al., 1973, Heredia et al., 1989 and Velando et al., 1973

2.5.2 Downplunge Projections

Surface map patterns of deformed terranes provide a distorted view of deformation patterns within the subsurface (Johnston, 1999). In our map area, where structures are plunging and topography represents less than 5% of the depth to which structures extend into the subsurface, it is appropriate to create downplunge projections in order to view structures in profile. By constructing downplunge projections of the folds that affect the

thrust sheets we are able to view the folds in profile, which allows us to better constrain fold geometry. As the folds in the thrust sheets are not cylindrical (i.e. the fold axes steepen toward the west and shallow with depth) we divide the map area into six smaller domains that can be treated as cylindrical. Downplunge projections were created for the Laviana, Rioseco and Campo de Caso thrust sheet (Figures 2 - 6, 2 - 7, 2 - 8, 2 - 9) by stitching together downplunge projections that were created for each of the six domains. The downplunge projections were created according to the method defined by Johnston (1999). Using downplunge projections of the steep, westward trending regional folds, we were able to calculate the amount of N-S shortening that each thrust sheet accommodated. Shortening was calculated by measuring the distance across the folds from hinge of the Beleño syncline to the hinge of the San Isidro anticline in each thrust sheet and comparing it with the measured restored length of the thrust sheets prior to folding. The length across the folds in the Laviana thrust sheet after folding is 10.6 km and the length of the thrust sheet prior to folding is 18.8 km. By dividing the difference of these measurements by the length of the restored thrust sheet we calculate that the Laviana thrust sheet was shortened by 44%. We used the same technique to calculate the shortening in the Rioseco and Campo de Caso thrust sheet. The distance across the folds of the Rioseco thrust sheet is 9 km, the restored length of the sheet is 21 km, and the shortening is 57%. The distance across the folds of the Campo de Caso thrust sheet is 8.8 km, the restored length of the sheet is 18.4 km, and the shortening is 52%. We also used the downplunge projections to measure the wavelength and amplitude of the folds. The wavelength and amplitude of the folds in the Laviana thrust sheet are 12 km and 3.5 km respectively. The wavelength and amplitude of the folds in the Rioseco thrust sheet are

11.6 km and 4.4 km respectively. We also observe that the folds become asymmetric in the younger, underlying, thrust sheets. These folds verge to the north as indicated by the northward dip of their axial planes.

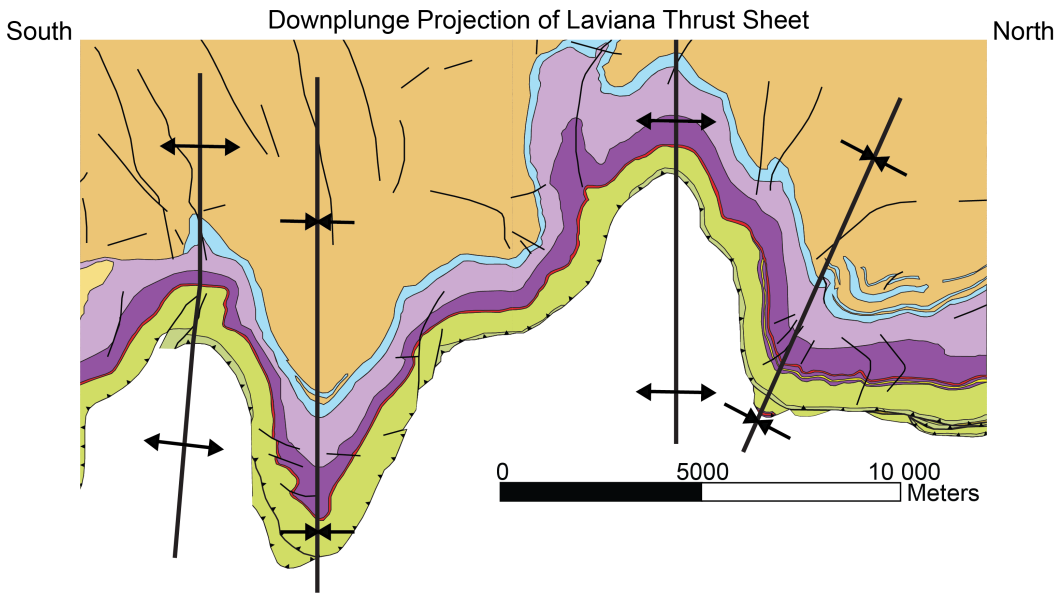

Figure 2 - 6 Downplunge Projection of the Laviana Thrust Sheet. Projected down the trend and plunge of 60º towards 266º. Calculated shortening according to measured distance across folds and measured restored length of thrusts is 44%. See Figure 2 - 3 for legend.

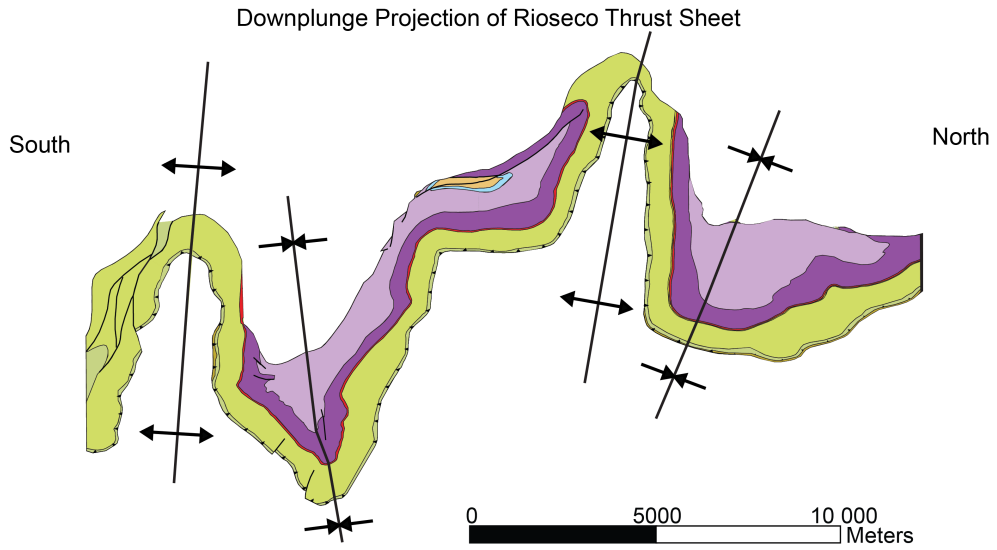

Figure 2 - 7 Downplunge Projection of the Rioseco Thrust Sheet. Projected down the trend and plunge of 41º towards 267º. Calculated shortening according to measured distance across folds and measured restored length of thrusts is 57%. See Figure 2 - 3 for legend.

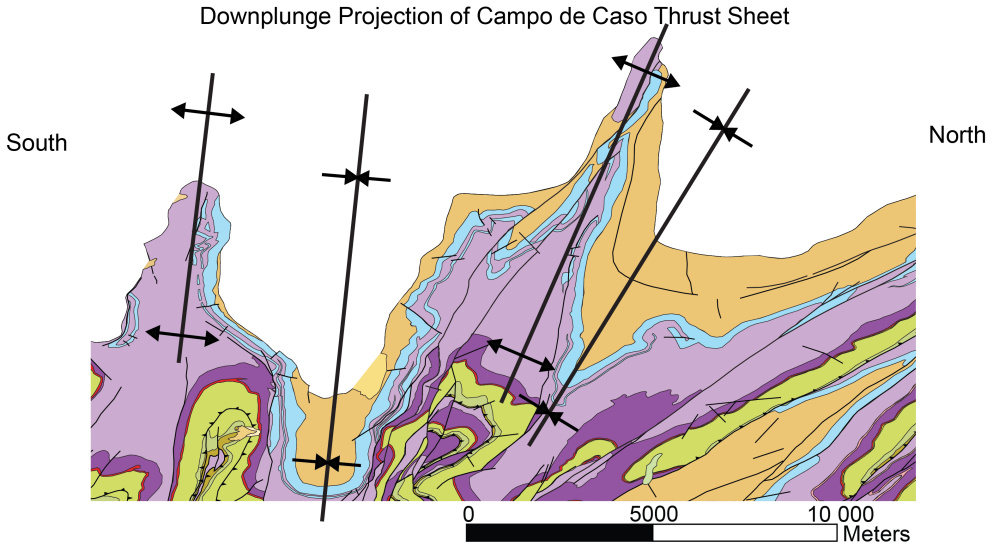

Figure 2 - 8 Downplunge Projection of the Campo de Caso Thrust Sheet. Projected down the trend and plunge of 33º towards 264º. Calculated shortening according to measured distance across folds and measured restored length of thrusts is 55%. See Figure 2 - 3 for legend.

2.5.3 Vertical Cross-Sections

We also created a line-length balanced (as per Dahlstrom, 1969) cross-section (Figure 2 - 10) that contains the average vector of thrust sheet emplacement, trending 090 degrees, in order to analyse the amount of shortening attributable to Variscan thrusting. We constructed this section along the hinge of the Tarna syncline in order to minimize the affects of post-Variscan folding. Line length was balanced using the base of the Barrios quartzite. This palinspastic cross-section indicates >16 km of shortening was taken up just by the Laviana and Rioseco thrust sheets, and is consistent with previous estimates of ~60 km of shortening (Alvarez-Marón and Pérez Estaún, 1988) accommodated by the fold and thrust belt in total. In addition, the cross-section shows that, along the axial plane of the Tarna syncline, the Rioseco thrust merges with the Laviana at a depth of ~4 km, implying 6 km of structural relief relative to the San Isidro anticline to the south and 9 km with respect to the Rio Monasterio anticline to the north, which is consistent with our downplunge projections (Figs 5, 6 and 7).

2.6 Interpretations and discussion

West-plunging folds of thrust faults and related fault-bend folds within the east-verging Cantabrian zone thrust belt of the Variscan orogen have been attributed to lateral ramps in underlying thrust faults (Alvarez-Marron and Perez-Estaun, 1988; Alvarez-Marrón, 1995). In this model, Ponga Unit folds are interpreted to result from displacement over lateral ramps in the underlying thrust faults during Variscan thrust imbrication. An alternative interpretation is that the folds are post-Variscan structures that overprinted the thrust belt. Our structural analysis of thrusts and folds in the Ponga Unit and detailed downplunge projections place constraints on the formation mechanism of the

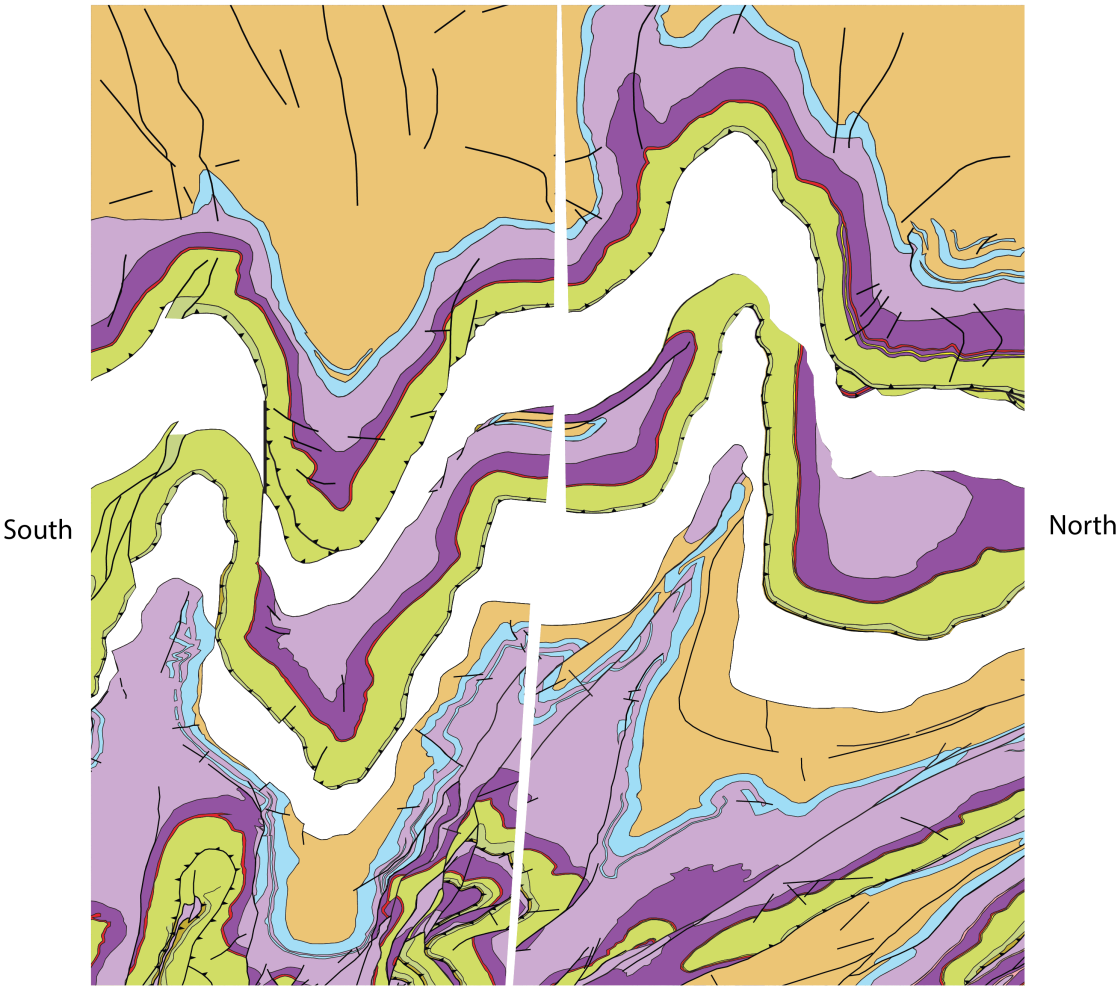

Figure 2 - 9 Combined downplunge projections of the Laviana, Rioseco and Campo de Caso thrust sheets. See Figure 2 - 3 for legend.

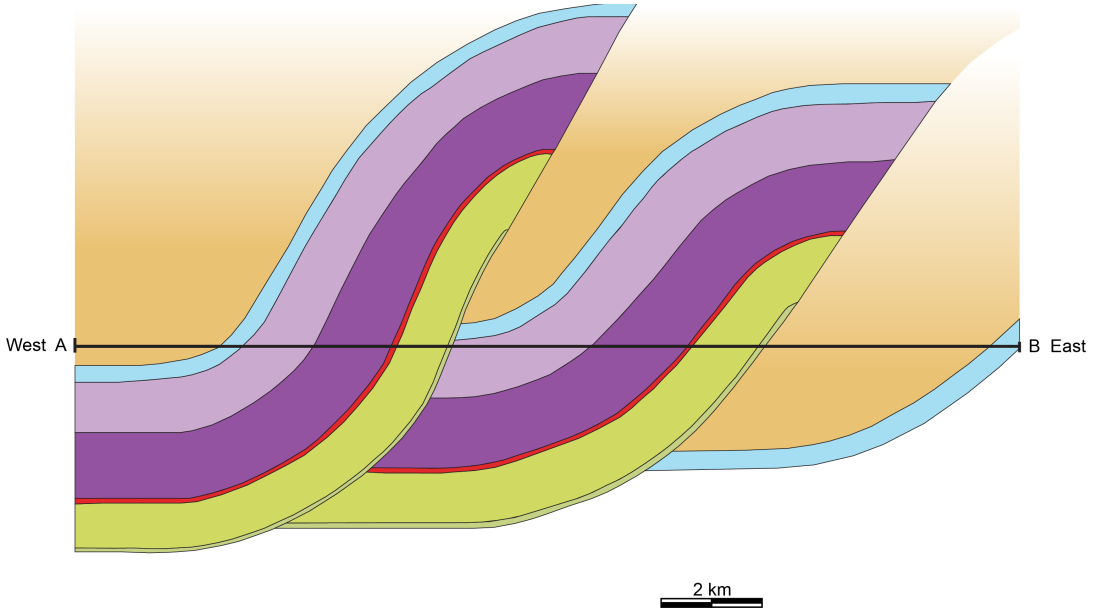

Figure 2 - 10 Cross section A-B is oriented to contain the vector of motion that describes thrust sheet emplacement. This section is balanced for only the Lavriana and Rioseco thrust sheets. See Figure 2 - 3 for legend.

west-plunging folds, as discussed further. We start with a brief review of the typical geometry of lateral-ramp related folds, then demonstrate how the geometry of the west-plunging folds is inconsistent with this model, and instead require superposed folding of the thrust belt. Finally, we comment on the significance of our findings for models of the hairpin Cantabrian orocline in the Variscan orogen of northern Iberia.

Lateral ramp related folds (Figure 2 - 11): (1) have axes that trend perpendicular to the thrust traces and plunge toward the hinterland; (2) are typically open, homoclinal with upright limbs, and verge along strike towards the thrust tips; (3) tend to converge into parallelism with fault-bend folds that are attributable to frontal ramps due to linking of lateral and frontal ramps through oblique structures; (4) are irregularly developed but are more commonly developed away from the center of the thrust sheet; (5) are restricted in

relief to be less than or equal to the height of the lateral ramps, restricting them to a maximum of a few kilometers of structural relief; and (6) typically result in minor to insignificant (no more than a few percent) orogen-parallel shortening of the thrust sheet. Classic examples of thrust sheets characterized by lateral-ramp related folds include the Moine Thrust Belt (Boyer and Elliott, 1982) and the Rundle Thrust (Wilkerson et al., 2002) among others.

Consistent with their interpretation as lateral-ramp related folds (Pérez-Estaún et al., 1988; Alvarez-Marrón, 1995), the west-plunging folds of the Ponga Unit trend perpendicular to the regional strike of the Ponga Unit thrust faults. They are, however, otherwise unlike lateral-ramp related folds. The folds plunge consistently westward without variation in plunge direction; oblique ramps are absent, and nowhere are the west-plunging folds observed to merge via oblique structures into fault-bend folds attributable to frontal ramps. The west-plunging folds are symmetric, not homoclinal, and are characterized by a regular, predictable pattern with consistent wavelengths and amplitudes throughout. Fold amplitudes average 3.5 km, and hence structural relief averages ~7 km. The structural relief exceeds the thickness of any of the Ponga Unit thrust sheets (Figure 2 - 10), and hence exceeds the maximum height of any possible Ponga Unit lateral ramp. Far from being open, the west-plunging folds are tight and locally isoclinal, and have steeply-dipping to locally overturned limbs. Their axial planes are vertical to steeply south dipping, yielding a consistent N-verging geometry. Steeply-plunging to vertical folds of the scaly Variscan cleavage developed in the siliciclastic units demonstrate that folding was post-Variscan and implies that the west-plunging folds were generated during buckling of the thrust belt about a vertical axis of rotation.

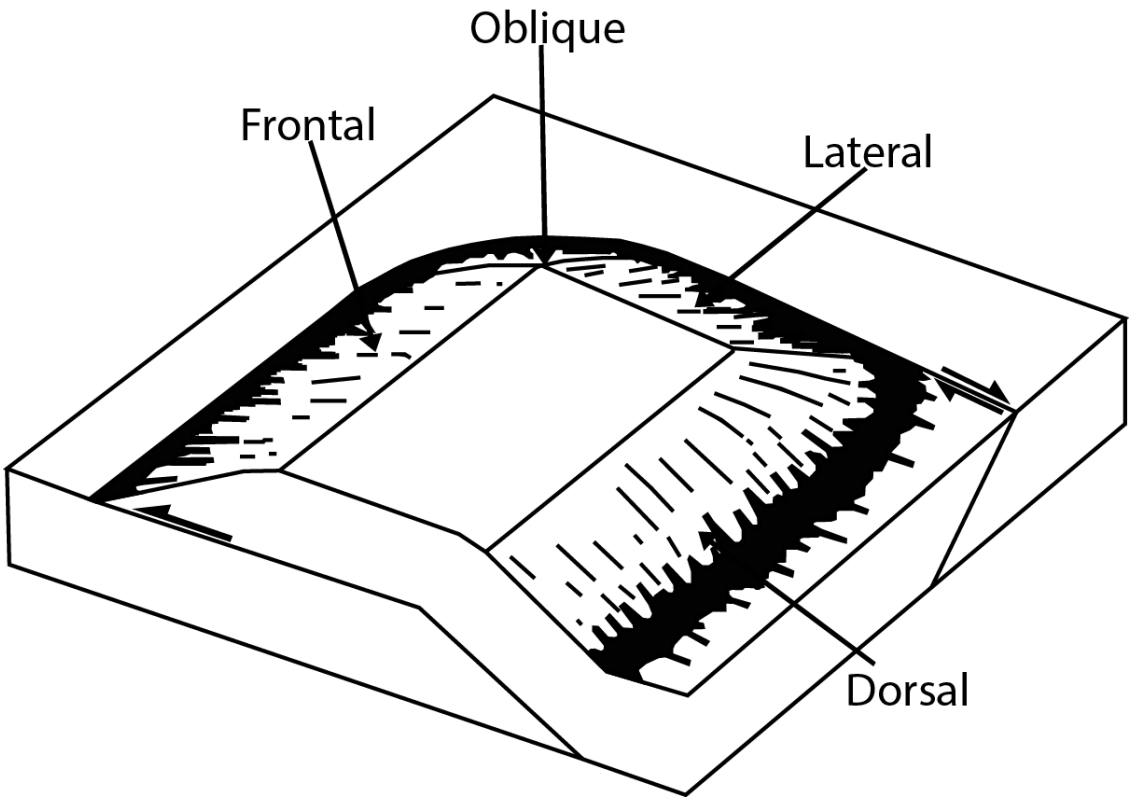

Figure 2 - 11 Figure shows characteristics of lateral ramp related folds. Lateral ramp related folds: 1) have folds axes trending perpendicular to thrust trace; 2) are open, homoclinal and verge along strike towards thrust tips, 3) converge into parallelism with fault bend folds that are attributable to frontal ramps; 4) are irregular with increasing likelihood to develop away from center of thrust sheet; 5) are restricted in relief and are found to be less than or equal to height of lateral ramps; and 6) typically result in minor to insignificant orogen-parallel shortening of the thrust sheet. Modified from Butler (1982).

Interpretation of the west-plunging folds as being superposed on the main post-Variscan thrusts implies that there were two distinct orogenic events. A testable prediction of this model is that folding of the Variscan fold and thrust belt should have

yielded a fold interference pattern (e.g. Ramsay and Huber, 1987). Indeed, the Ponga Unit map pattern resembles a classic mushroom-type fold interference pattern (Figure 2 - 12). Geometric modeling shows that mushroom-type fold interference patterns result from successive deformation events characterized by principal compressive stresses at a high angle or even perpendicular to each other (Ramsay Type 2) (Figure 2 - 12c). Recognition of the Ponga Unit mushroom-type fold interference pattern is attributable to

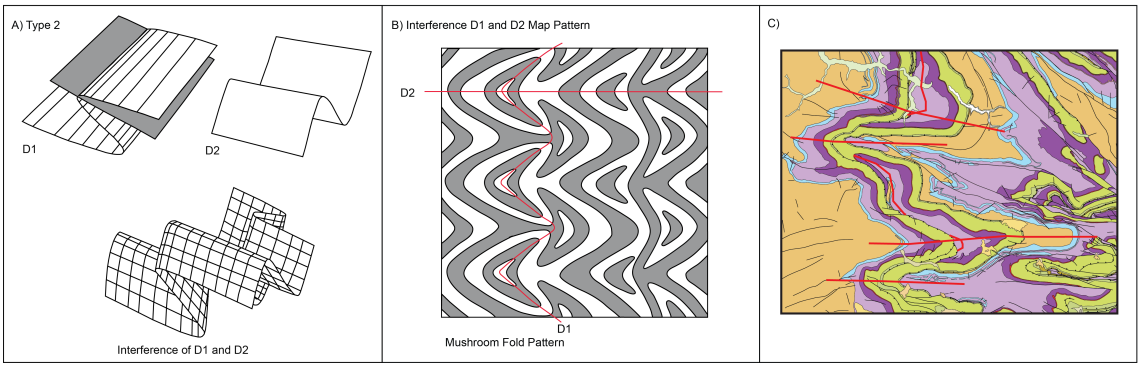

Figure 2 - 12 Ramsay Type 2 interference pattern. A) Mushroom fold patterns are formed from the interference of two distinct fold sets with axial planes oriented at high angle to one another. B) Typical mushroom fold interference pattern displaying hinge lines from the first (D1), and second (D2) deformation events. C) Interpreted D1 and D2 hinge lines overlain on the geological map of the study area. Map area resembles mushroom fold pattern obscured by thrust sheets. Modified from: A) Ramsay and Huber (1987); and B) Alvarez-Marrón et al. (1990), Caride et al. (1973),Heredia et al. (1989) and Velando et al. (1973). See Figure 2 - 3 for legend.

Julivert and Marcos (1973). The mushroom-type interference pattern represents a positive test for a model of the west-plunging folds as products of orogen-parallel principal compressive stress after Variscan fold and thrust belt development. An additional argument in favour of superposed folding is that our data show a progressive steepening of fold axes towards the west (Figure 2 - 4), which is predicted in a typical fold and thrust belt where folds and bedding progressively steepen towards the metamorphic hinterland. A superposed perpendicular shortening event will create a second generation of folds that also progressively steepen toward the hinterland which is observed in the field area. Oroclinal buckling resulted in local thrust reactivation and the development of numerous brittle and brittle-ductile strike-slip faults with complex movement histories within the orocline hinge region. These steeply-dipping faults accommodated tangential shortening during oroclinal buckling (Weil et al., 2013; Gutierrez-Alonso et al., 2015).

Paleomagnetic data have been used to argue that the west-plunging folds are at least in part attributable to lateral ramps. Declination data from a secondary 'B' remanence magnetization (Weil et al., 2013a) show deflections from a regional magnetic trend that were attributed to a post-remanence, but pre-oroclinal folding that Weil (2006) interpreted as Variscan deformation related to lateral and oblique ramps in the Ponga Unit thrust faults. Our structural study shows that the west-plunging folds are unlikely to be related to lateral ramps, are instead better interpreted as the result of post-Variscan deformation, and this suggests that an alternative interpretation of the paleomagnetic data should be entertained.

The age of the secondary 'B' remanence is "latest Stephanian to Early Permian, after initial D1 thrusting but prior to major secondary rotation" (Weil, 2006, p.1). However,

the constraints on the timing of oroclinal bending are commonly given as being Stephanian to Early Permian (see for example Gutiérrez-Alonso et al., 2012; and Weil et al., 2013b, their Figure 7). The extreme age constraints provided by the Paleomagnetic and structural data (beginning of the Stephanian at 304 Ma to the end of the Sakmarian at 294 Ma indicates that a maximum of 10 m.y. separates the end of Variscan thrusting and orocline formation. We suggest that instead of overlapping with and recording deformation attributable to Variscan thrusting (as per Weil, 2006), the 'B' remanence in the Ponga Unit likely post-dates Variscan deformation and overlaps with and records initial deformation attributable to oroclinal buckling. Our interpretation is consistent with the 'B' remanence being an entirely post-Variscan remanence, as it is to the west of the Ponga Unit (Weil, 2006); this interpretation is compatible with the available paleomagnetic and structural age constraints described above. Weil (personal communication, 2016) has suggested that the Ponga Unit magnetization is not the 'B' magnetization recorded west of the study area, but is a 'B2' magnetization that was acquired later, during early oroclinal bending. Syn-deformation magnetization can be protracted and have systematic spatial acquisition, with more recent magnetization acquisition the farther one progresses into the foreland (e.g. Enkin et al., 1997). Interpretation of the onset of Cantabrian orocline formation as being immediately post-Variscan and overlapping with a 'B2' magnetization within the Variscan foreland reconciles structural and paleomagnetic data within the Ponga Unit, confirms the latest Stephanian to earliest Permian onset of oroclinal buckling, and implies that the switch from Variscan deformation to oroclinal buckling was geologically instantaneous.

A secondary orocline model for the Cantabrian orocline requires a post-Variscan change in the orientation of the principal compressive stress from orogen-perpendicular to orogen-parallel (Gutiérrez-Alonso et al., 2012; Johnston et al., 2013; Weil et al., 2013b). Our analysis shows that west-plunging folds of the Ponga Unit affected the Variscan thrust faults, and formed in response to an orogen-parallel principal compressive stress. Either the stress field rotated 90 degrees about a vertical axis of rotation, or the maximum and intermediate stress axes, both of which lay in the horizontal plane, switched places. Either way, the principal compressive stress switched from an orogen-perpendicular orientation to an orogen-parallel orientation (Pastor-Galan et al., 2015). Our findings are congruent with the Cantabrian orocline being a true orocline formed by buckling of pre-existing linear structures. Furthermore, paleomagnetic data record the onset of orocline-related folding immediately after the cessation of Variscan orogenesis, providing only a small window of time between the end of Variscan orogenesis and the beginning of oroclinal buckling (Johnston et al., 2013).

2.7 Conclusion

We investigated the complex fold pattern of the Ponga Unit in the hinge of the Cantabrian orocline in order to test Progressive versus Secondary models of orocline formation. Our data show that the observed map pattern is attributable to post-Variscan folding of the Cantabrian fold and thrust belt in response to an orogen-parallel principal compressive stress. The post-Variscan deformation that we describe is consistent with the predications of models of the Cantabrian orocline as a secondary orocline. Timing constraints provided by paleomagnetic data indicate that orocline formation began immediately after the cessation of Variscan deformation.

2.8 Acknowledgements

Research was supported by a University of Victoria Graduate Studies Award and an Natural Sciences and Engineering Research Council of Canada (NSERC) Discovery Grant to Stephen T. Johnston. Arlo Weil is thanked for helping us understand and interpret the paleomagnetic data from the Ponga Unit. Theron Finley is thanked for his tireless efforts as a field assistant. Insightful and constructive reviews provided by Domingo Aerden and an anonymous reviewer significantly improved the manuscript.

Chapter 3. Conclusion

3.1 Conclusions

The goal of this thesis was to evaluate the structure at the core of the Cantabrian orocline in order to further assess how the Cantabrian orocline formed. We addressed this goal by examining map scale, west-plunging folds located in the Ponga Unit, a tectonostratigraphic package within the Variscan foreland fold and thrust belt. We compared two end-member models for the formation of the Ponga Unit folds, one that relates them to lateral ramps in Variscan thrust faults, and one that relates them to secondary deformation during post-Variscan oroclinal buckling. The main conclusions of this thesis are:

(1) The geometry of the west-plunging folds of the Ponga Unit is inconsistent with a lateral-ramp related fold interpretation. Like lateral-ramp related folds, the west-plunging folds of the Ponga Unit trend perpendicular to regional strike of the thrust belt. They are, however, otherwise quite unlike lateral-ramp related folds, being: characterized by a consistent wavelength and amplitude; distinguished by a structural relief that is in excess of the maximum height of any possible lateral ramp; and tight and asymmetric yielding a N-verging geometry.

(2) The fold pattern of the Ponga Unit resembles a mushroom fold interference pattern that it is likely the result of two deformation phases including secondary, orocline-related, N-S shortening immediately after the cessation of E-W Variscan shortening.

(3) Although paleomagnetic data has previously been used to argue that the west-plunging folds of the Ponga Unit are in part attributable to lateral ramps, we find that the 'B' remanence in the Ponga Unit likely overlaps in time with the cessation of Variscan deformation and records post-Variscan deformation associated with the onset of oroclinal buckling.

3.2 Recommendations for further work

The findings presented in this thesis point to new research questions, the pursuit of which will enable further development and testing of a model for secondary orocline formation.

Johnston et al. (2013) were the first to suggest that secondary oroclines formation occurs within a relatively narrow time window immediately following the cessation of regional orogenesis. They suggested that the reason for this limited 'window of opportunity' may be that mantle tectonized during orogenesis subsequently anneals and attains thermal and gravitational equilibrium. Therefore, there may be only a short interval between the end of orogenesis and the subsequent stabilization of the lithospheric mantle available for secondary orocline formation. This interpretation suggests that unless an orogen-parallel stress develops within that window of opportunity, oroclines will not form and implies that secondary orocline formation is 'opportunistic'.

I have shown that initiation of the formation of the Cantabrian orocline overlapped with remagnetization attributable to Variscan orogenesis. These findings suggest that the onset of orocline formation is not 'opportunistic,' but is a product of the same processes responsible for the termination of orogenesis. Is this a relationship that is uniformly

characteristic of all secondary oroclines? If so, why? What plate tectonic setting or settings could possibly explain this linkage?

Timing of orocline formation has been best constrained in the Cantabrian orocline relative to other oroclines. Focused geochronologial-paleomagnetic studies on other oroclines, for example the Carpathian Balkan, the Olympic or the Alaskan oroclines could be important in constraining the relationship between the end of orogenesis and the initiation of oroclinal buckling. However, the caveat is such that studies require good exposure for paleomagnetic sampling, and accessible syn-tectonic sedimentary sequences in order to constrain timing relationships. The Olympic orocline is well exposed, however much of the exposed rock consists of thick sequences of pillow basalts in which paleohorizontal is difficult to ascertain, reducing the suitability of these rocks for a paleomagnetic study (Beck and Engebretson, 1982). The Carpathian-Balkan oroclines are heavily eroded and exposure is poor. The Alaskan oroclines are remote and difficult and expensive to access.

Well developed thrust belts are inferred to occur within retro- and forearc settings suggesting that orocline formation if not necessarily limited to a specific tectonic setting. We have shown that a classic mushroom-style (Ramsay type 2) fold interference pattern is the result of orocline formation. This begs the question: are such type 2 fold interference patterns diagnostic of oroclines, and are they characteristic of oroclines affecting thrust belts that verge toward the orocline core. Oroclines have commonly been overlooked in regional mapping projects and it is possible that type-2 interference patterns point to the presence of oroclines that have been previously overlooked. In this instance, poor exposure is not a limitation. First order studies could be done with lidar

surveying and analysis followed up by detailed structural studies similar to the one reported on here. Lidar may be particularly useful in identifying younger oroclines. Mapping focused on type-2 fold interference patterns exposed in ancient continental shields and cratons could test for Precambrian oroclines (Lahtinen et al., 2014). A particular focus on the oroclines in the Canadian Shield may also help test the suggestion that shield formation and the beginning of continental growth involved oroclinal buckling of arcs and ribbon continents (Johnston, 2001; Van der Voo, 2004).

The finding that a mushroom-style interference pattern characterizes a thrust belt that verges toward the orocline core, as in the case of the Cantabrian orocline, suggests that further investigation should go into determining if other oroclines are characterized by similar type-2 interference fold patterns. Oroclines to investigate could include: the Kulukbuk Hills orocline, the southern member of the coupled Alaskan oroclines (Johnston, 2001; Bradley et al., 2003); the Balkan orocline, the southern member of the coupled Carpathian/Alpine oroclines (Shaw and Johnston, 2012); or the southerly member of the Bothnian oroclines (Lahtinen et al., 2014).

The Cantabrian orocline is the northern member of a pair of coupled oroclines (Shaw and Johnston, 2012). The convex to the west Cantabrian orocline preserves the non-metamorphosed Cantabrian fold and thrust belt within its core (Julivert, 1971). Variscan folds and faults verge toward the core of the Cantabrian orocline, and the core of the orocline is characterized by shallow crustal deformation involving refolding of the fold and thrust belt during orocline formation. The core of the southern member of the coupled Iberian oroclines, the Central Iberian orocline, is convex to the east and preserves the crystalline meta-plutonic hinterland of the Variscan orogen within its core,

as well as obducted oceanic terranes emplaced during orogenesis (Shaw et al., 2012). The prediction developed here, which needs to be tested by a detailed structural mapping study, is that the core of the southern, Central Iberian orocline should be characterized by Variscan structures that verge away from the orocline core. One way to test this prediction is to do a kinematic strain analysis study on the core of the Central Iberian orocline. Another question that arises is what, if any, orocline-related structures characterize the core region of the Central Iberian orocline.

Major Variscan structures along the south limb of the Central Iberian orocline, such as the sinistral Badajoz-Cordoba shear zone, and the Beja Abuches ophiolite (Figure 1 - 2), should wrap around the Central Iberian orocline and be continuous into the core region of the Cantabrian orocline. Mapping and structural analyses, as well as regional mapping of the Cantabrian orocline, have failed to identify the northern continuation of these structures. Additional detailed mapping, similar to this study, extending to the southeast along the southern limb of the Cantabrian orocline may help determine if these structures are continuous around the Central Iberian orocline and into the Cantabrian orocline.

References

Aerden, D.G.A.M., 2004, Correlating deformation in Variscan NW-Iberia using porphyroblasts; implications for the Ibero-Armorican Arc: Journal of Structural Geology, v. 26, p. 177–196.

Allmendinger, R.W., Cardozo, N., and Fisher, D.M., 2011, Structural geology algorithms: Vectors and tensors in structural geology: Cambridge University Press, 302 p.

Alvarez Marrón, J., 1989, La estructura de la región del Ponga (Zona Cantábrica, NW de España). PhD Thesis, Universidad de Oviedo (London).

Alvarez-Marrón, J., 1995, Three-dimensional geometry and interference of fault-bend folds: examples from the Ponga Unit, Variscan Belt, NW Spain: Journal of Structural Geology, v. 17, p. 549–560, doi: 10.1016/0191-8141(94)00075-B.

Alvarez-Marron, J., and Perez-Estaun, A., 1988, Thin skinned tectonics in the Ponga region (Cantabrian Zone, NW Spain): Geologische Rundschau, v. 77, p. 539–550, doi: 10.1007/BF01832397.

Alvarez-Marrón, J., Pérez-Estaun, A., Aller, N., and Heredia, N.S., 1990, Mapa Geologico de España, Puebla de Lillo: Madrid S.A. Mapa Geologico de España, http://info.igme.es/cartografia/datos/magna50/jpg/d0_jpg/Editado_MAGNA50_79.jpg (accessed June 2014).

Bahamonde, J.R., 1990, Estratigrafía y Sedimentología del Carbonífero medio y superior de la Región del Manto del Ponga (Zona Cantábrica), PhD Thesis, Universidad de Oviedo, Oviedo, Spain, 38 p.

Bahamonde, J.R., and Colmenero, J.R., 1993, Análisis estratigráfico del Carbonífero medio y superior del Manto del Ponga (Zona Cantábrica): Trabajos de Geología, Oviedo, v. 19, p. 155–193.

Beck, M.E., and Engebretson, D.C., 1982, Paleomagnetism of small basalt exposures in the West Puget Sound Area, Washington, and Speculations on the accretionary origin of the Olympic Mountains: Journal of Geophysical Research: Solid Earth, v. 87, p. 3755–3760, doi: 10.1029/JB087iB05p03755.

Boyer, S.E., and Elliott, D., 1982, Thrust systems: AAPG Bulletin, v. 66, p. 1196–1230.

Bradley, D.C., Dumoulin, J., Layer, P., Sunderlin, D., Roeske, S., McClelland, B., Harris, A.G., Abbott, G., Bundtzen, T., and Kusky, T., 2003, Late Paleozoic orogeny in Alaska's Farewell terrane: Tectonophysics, v. 372, p. 23–40.

Brun, J.-P., and Burg, J.-P., 1982, Combined thrusting and wrenching in the Ibero-Armorican arc: A corner effect during continental collision: Earth and Planetary Science Letters, v. 61, p. 319–332, doi: 10.1016/0012-821X(82)90063-2.

Butler, R.W.H., 1982, The terminology of structures in thrust belts: Journal of Structural Geology, v. 4, p. 239–245, doi: 10.1016/0191-8141(82)90011-6.

Caride, C., Gevilla, M., Ortuño, G., and Velando, F., 1973, Mapa Geologico de España, Mieres: Servicio de Publicaciones - Ministerio de Industria Mapa Geologico de España, http://info.igme.es/cartografia/datos/magna50/jpg/d0_jpg/Editado_MAGNA50_53.jpg (accessed June 2014).

Colmenero, J.R., Fernández, L.P., Moreno, C., Bahamonde, J.R., Barba, P., Heredia, N., and González, F., 2002, Carboniferous, *in* Gibbons, W., and Moreno, T., eds., The Geology of Spain: London, Geological Society of London, p. 93–116.

Dahlstrom, C.D.A., 1969, Balanced cross sections: Canadian Journal of Earth Sciences, v. 6, p. 743–757, doi: 10.1139/e69-069.

Enkin, R.J., Wheadon, P.M., Baker, J., and Osadetz, K.G., 1997, Paleomagnetic constraints on the tectonic history of the Foreland Belt, southern Canadian Cordillera: preliminary results: Canadian Journal of Earth Sciences, v. 34, p. 260–270, doi: 10.1139/e17-024.

Gallastegui, J., Pulgar, J.A., and Alvarez-Marrón, J., 1997, 2-D seismic modeling of the Variscan foreland thrust and fold belt crust in NW Spain from ESCIN-1 deep seismic reflection data: Tectonophysics, v. 269, p. 21–32, doi: 10.1016/S0040-1951(96)00166-7.

Gutiérrez-Alonso, G., Fernández-Suárez, J., Gutiérrez-Marco, J.C., Corfu, F., Murphy, J.B., and Suárez, M., 2007, U-Pb depositional age for the upper Barrios Formation (Armorican Quartzite facies) in the Cantabrian zone of Iberia: Implications for stratigraphic correlation and paleogeography, *in* Linnemann, U., Nance, R.D., Kraft, P., and Zulauf, G., eds., The Evolution of the Rheic Ocean: From Avalonian-Cadomian Active Margin to Alleghenian-Variscan Collision, Volume 423: Boulder, CO, United States (USA), Geological Society of America (GSA), p. 287-296

Gutiérrez-Alonso, G., Fernández-Suárez, J., Weil, A.B., Brendan Murphy, J., Damian Nance, R., Corfú, F., and Johnston, S.T., 2008, Self-subduction of the Pangaean global plate: Nature Geoscience, v. 1, p. 549–553, doi: 10.1038/ngeo250.

Gutiérrez-Alonso, G., Johnston, S.T., Weil, A.B., Pastor-Galán, D., and Fernández-Suárez, J., 2012, Buckling an orogen: the Cantabrian Orocline: GSA Today, v. 22, no. 7, p. 4–9.

Gutiérrez-Alonso, G., Collins, A.S., Fernández-Suárez, J., Pastor-Galán, D., González-Clavijo, E., Jourdan, F., Weil, A.B., and Johnston, S.T., 2015, Dating of lithospheric buckling: 40Ar/39Ar ages of syn-orocline strike–slip shear zones in northwestern Iberia: Tectonophysics, v. 643, p. 44–54, doi: 10.1016/j.tecto.2014.12.009.

Gutiérrez-Marco, J.C., Robardet, M., Rábano, I., Sarmiento, G.N., San José Lancha, M.Á., and Herranz, P.A., 2002, Ordovician, in Gibbons, W., and Moreno, T., eds., The Geology of Spain: London, The Geological Society.

Heredia, N., and Rodriguez Fernández, L.R., 1989, Mapa Geologico de España, Rioseco: Madrid S.A. Mapa Geologico de España, http://info.igme.es/cartografia/datos/magna50/jpg/d0_jpg/Editado_MAGNA50_54.jpg (accessed June 2014).

Hirt, A.M., Lowrie, W., Julivert, M., and Arboleya, M.L., 1992, Paleomagnetic results in support of a model for the origin of the Asturian Arc: Tectonophysics, v. 213, p. 321–339.

Johnston, S.T., 1999, Squeezing down plunge projections out of graphics packages: Computers & Geosciences, v. 25, p. 197–200, doi: 10.1016/S0098-3004(98)00118-6.

Johnston, S.T., 2001, The Great Alaskan Terrane Wreck: reconciliation of paleomagnetic and geological data in the northern Cordillera: Earth and Planetary Science Letters, v. 193, p. 259–272.

Johnston, S.T., Weil, A.B., and Gutiérrez-Alonso, G., 2013, Oroclines: Thick and thin: Geological Society of America Bulletin, v. 125, p. 643–663, doi: 10.1130/B30765.1.

Julivert, M., 1971, Décollement tectonics in the Hercynian Cordillera of northwest Spain: American Journal of Science, v. 270, p. 1–29, doi: 10.2475/ajs.270.1.1.

Julivert, M., and Arboleya, M.L., 1984, A geometrical and kinematical approach to the nappe structure in an arcuate fold belt: the Cantabrian nappes (Hercynian chain, NW Spain): Journal of Structural Geology, v. 6, p. 499–519, doi: 10.1016/0191-8141(84)90061-0.

Julivert, M., and Marcos, A., 1973, Superimposed folding under flexural conditions in the Cantabrian Zone (Hercynian Cordillera, northwest Spain): American Journal of Science, v. 273, p. 353–375, doi: 10.2475/ajs.273.5.353.

Lahtinen, R., Johnston, S.T., and Nironen, M., 2014, The Bothnian coupled oroclines of the Svecofennian Orogen: a Palaeoproterozoic terrane wreck: Terra Nova, v. 26, p. 330–335.

Lefort, J.-P., 1979, Iberian-Armorican arc and Hercynian orogeny in western Europe: Geology, v. 7, p. 384–388, doi: 10.1130/0091-7613(1979)7<384:IAAHOI>2.0.CO;2.

Marshak, S., and Tabor, J.R., 1989, Structure of the Kingston orocline in the Appalachian fold-thrust belt, New York: Geological Society of America Bulletin, v. 101, no. 5, p. 683–701, doi: 10.1130/0016-7606(1989)101<0683:SOTKOI>2.3.CO;2.

Martínez-Catalán, J., 1990, A non-cylindrical model for the northwest Iberian allochthonous terranes and their equivalents in the Hercynian belt of Western Europe: Tectonophysics, v. 179, p. 253–272, doi: 10.1016/0040-1951(90)90293-H.

Martínez Catalán, J.R., 2011, Are the oroclines of the Variscan belt related to late Variscan strike-slip tectonics?: Terra Nova, v. 00, p. 1-7.

Merino-Tomé, O.A., Bahamonde, J.R., Colmenero, J.R., Heredia, N., Villa, E., and Farias, P., 2009, Emplacement of the Cuera and Picos de Europa imbricate system at the core of the Iberian-Armorican arc (Cantabrian zone, north Spain): New precisions concerning the timing of arc closure: Geological Society of America Bulletin, v. 121, p. 729–751.

Murphy, J.B., Quesada, C., Gutiérrez-Alonso, G., Johnston, S.T., and Weil, A., 2016, Reconciling competing models for the tectono-stratigraphic zonation of the Variscan orogen in Western Europe: Tectonophysics, v. 681, p. 209–219, doi: 10.1016/j.tecto.2016.01.006.

Nance, R.D., Gutiérrez-Alonso, G., Keppie, J.D., Linnemann, U., Murphy, J.B., Quesada, C., Strachan, R.A., and Woodcock, N.H., 2010, Evolution of the Rheic Ocean: Gondwana Research, v. 17, p. 194–222, doi: 10.1016/j.gr.2009.08.001.

Parés, J.M., Van der Voo, R., Stamatakos, J., and Pérez-Estaún, A., 1994, Remagnetizations and postfolding oroclinal rotations in the Cantabrian/Asturian arc, northern Spain: Tectonics, v. 13, p. 1461–1471, doi: 10.1029/94TC01871.

Pastor-Galán, D., Groenewegen, T., Brouwer, D., Krijgsman, W., and Dekkers, M.J., 2015, One or two oroclines in the Variscan orogen of Iberia? Implications for Pangea amalgamation: Geology, v. 43, p. 527–530, doi: 10.1130/G36701.1.

Pastor-Galán, D., Gutuérrez-Alonso, G., and Weil, A.B., 2011, Orocline timing through joint analysis: Insights from the Ibero-Armorican Arc: Tectonophysics, v. 507, p. 31–46, doi: 10.1016/j.tecto.2011.05.005.

Pérez-Estaún, A., Bastida, F., Alonso, J.L., Marquínez, J., Aller, J., Alvarez-Marrón, J., Marcos, A., and Pulgar, J.A., 1988, A thin-skinned tectonics model for an arcuate fold and thrust belt: The Cantabrian Zone (Variscan Ibero-Armorican Arc): Tectonics, v. 7, p. 517–537.

Pérez-Estaún, A., Pulgar, J.A., Banda, E., and Alvarez-Marrón, J., 1994, Crustal structure of the external variscides in northwest spain from deep seismic reflection profiling: Tectonophysics, v. 232, p. 91–118, doi: 10.1016/0040-1951(94)90078-7.

Pérez-Estaún, A., Pulgar, J.A., Alvarez-Marrón, J., Dañobeitia, J.J., Gallastegui, J., Martínez-Catalán, J.R., Banda, E., Comas, M.C., and Córdoba, D., 1995, Results from the ESCI-N4 marine deep seismic profile in the northern Iberian Margin: Revista de la Sociedad Geológica de España, v. 8, p. 355–363.

Ramsay, J.G., 1962, The geometry of conjugate fold systems: Geological Magazine, v. 99, p. 516–526.

Ramsay, J.G., and Huber, M.I., 1987, The Techniques of Modern Structural Geology: Folds and Fractures: San Diego, California, Academic Press, 414 p.

Ribeiro, A., Dias, R., and Brandao Silva, J., 1995, Genesis of the Ibero-Armorican arc: Geodinamica Acta, v. 8, p. 173–184.

Ribeiro, A., Munhá, J., Dias, R., Mateus, A., Pereira, E., Ribeiro, L., Fonseca, P., Araújo, A., Oliveira, T., Romão, J., Chaminé, H., Coke, C., and Pedro, J., 2007, Geodynamic evolution of the SW Europe Variscides: Tectonics, v. 26, p. TC6009, doi: 10.1029/2006TC002058.

Ries, A.C., and Shackleton, R.M., 1976, Patterns of Strain Variation in Arcuate Fold Belts: Philosophical Transactions of the Royal Society of London A: Mathematical, Physical and Engineering Sciences, v. 283, p. 281–288, doi: 10.1098/rsta.1976.0085.

Shaw, J., and Johnston, S.T., 2012, The Carpathian-Balkan bends: An oroclinal record of ongoing Arabian–Eurasian collision, *in* (Eds.) Stephen Johnston and Gideon Rosenbaum, *Journal of the Virtual Explorer*, volume 43, paper 4, doi: 10.3809/jvirtex. 2012.00310 .

Shaw, J., and Johnston, S.T. Oroclinal buckling of the Armorican ribbon continent: An alternative tectonic model for Pangean amalgamation and Variscan orogenesis. In review: Lithosphere, v. Van der Pluijm Special Volume.

Shaw, J., Johnston, S.T., Gutiérrez-Alonso, G., and Weil, A.B., 2012, Oroclines of the Variscan orogen of Iberia: Paleocurrent analysis and paleogeographic implications: Earth and Planetary Science Letters, v. 329–330, p. 60–70, doi: 10.1016/j.epsl.2012.02.014.

Shaw, J., Gutiérrez-Alonso, G., Johnston, S.T., and Galán, D.P., 2014, Provenance variability along the Early Ordovician north Gondwana margin: Paleogeographic and tectonic implications of U-Pb detrital zircon ages from the Armorican

Quartzite of the Iberian Variscan belt: Geological Society of America Bulletin, v. 126, p. 702–719, doi: 10.1130/B30935.1.

Stewart, S.A., 1995, Paleomagnetic analysis of fold kinematics and implications for geological models of the Cantabrian/Asturian arc, north Spain: Journal of Geophysical Research: Solid Earth, v. 100, p. 20079–20094.

Suess, E., 1909, The Face of the Earth, translated from German (Suess, E., 1885. Das antlitz der erde. F. Tempsky, Vienna) by H.B.C. Sollas and W.J. Sollas: Oxford, Clarendon, 672 p.

Velando, F., Castello, R., and Orriz, F., 1973, Mapa Geologico de España, Pola de Lena: Servicio de Publicaciones - Ministerio de Industria Mapa Geologico de España, http://info.igme.es/cartografia/datos/magna50/jpg/d0_jpg/Editado_MAGNA50_78.jpg (accessed June 2014).

Van der Voo, R., 2004, Paleomagnetism, oroclines, and growth of the continental crust: GSA Today, v. 14, p. 4–9.

Van der Voo, R., Stamatakos, J.A., and Parés, J.M., 1997, Kinematic constraints on thrust-belt curvature from syndeformational magnetizations in the Lagos del Valle syncline in the Cantabrian Arc, Spain: Journal of Geophysical Research: Solid Earth (1978–2012), v. 102, p. 10105–10119, doi: 10.1029/97JB00263.

Weil, A.B., 2006, Kinematics of orocline tightening in the core of an arc: Paleomagnetic analysis of the Ponga Unit, Cantabrian Arc, northern Spain: Tectonics, v. 25, p. TC3012, doi: 10.1029/2005TC001861.

Weil, A.B., Van der Voo, R., Van der Pluijm, B.A., and Parés, J.M., 2000, The formation of an orocline by multiphase deformation: a paleomagnetic investigation of the Cantabria–Asturias Arc (northern Spain): Journal of Structural Geology, v. 22, p. 735–756.

Weil, A.B., Van der Voo, R., and Van der Pluijm, B.A., 2001, Oroclinal bending and evidence against the Pangea megashear: The Cantabria-Asturias arc (northern Spain): Geology, v. 29, p. 991–994.

Weil, A.B., Yonkee, A., and Sussman, A., 2010, Reconstructing the kinematic evolution of curved mountain belts: A paleomagnetic study of Triassic red beds from the Wyoming salient, Sevier thrust belt, USA: Geological Society of America Bulletin, v. 122, p. 3–23.

Weil, A.B., Gutiérrez-Alonso, G., and Wicks, D., 2013a, Investigating the kinematics of local thrust sheet rotation in the limb of an orocline: a paleomagnetic and structural analysis of the Esla tectonic unit, Cantabrian–Asturian Arc, NW Iberia: International Journal of Earth Sciences, v. 102, p. 43–60.

Weil, A.B., Gutiérrez-Alonso, G., Johnston, S.T., and Pastor-Galán, D., 2013b, Kinematic constraints on buckling a lithospheric-scale orocline along the northern margin of Gondwana: A geologic synthesis: Tectonophysics, v. 582, p. 25–49, doi: 10.1016/j.tecto.2012.10.006.

Wilkerson, S.M., Apotria, T., and Farid, T., 2002, Interpreting the geologic map expression of contractional fault-related fold terminations: lateral/oblique ramps versus displacement gradients: Journal of Structural Geology, v. 24, p. 593–607, doi: 10.1016/S0191-8141(01)00111-0.

Appendix

Table A - 1 Station, location and orientations of bedding measurements

Station	Easting	Northing	Dip	Dip Direction
PO-KD-001	302939	4773324	80	184
PO-KD-002	303073	4773307	75	168
PO-KD-003	303226	4773381	75	172
PO-KD-004	303366	4773378	85	158
PO-KD-005	303522	4773410	80	283
PO-KD-006	303555	4773433	58	238
PO-KD-006	303555	4773433	58	262
PO-KD-006	303555	4773433	78	210
PO-KD-006	303555	4773433	52	272
PO-KD-007	303633	4773519	80	162
PO-KD-008	303676	4773655	70	186
PO-KD-009	303727	4773636	62	238
PO-KD-010	303490	4773779	37	28
PO-KD-011	303415	4773794	75	233
PO-KD-012	303262	4773994	57	250
PO-KD-013	303229	4774050	60	210
PO-KD-014	303257	4774011	82	304
PO-KD-015	303225	4773886	85	282
PO-KD-016	303192	4773733	35	220
PO-KD-017	303194	4773648	60	264
PO-KD-018	303064	4773581	62	285
PO-KD-020	295939	4776163	45	22
PO-KD-021	296152	4776141	32	24
PO-KD-022	296207	4776261	62	366
PO-KD-023	296311	4776253	72	16
PO-KD-024	296396	4776446	90	0
PO-KD-026	296530	4776530	60	28
PO-KD-029	296388	4777073	75	192
PO-KD-030	296939	4777011	65	226
PO-KD-030	296939	4777011	65	230
PO-KD-031	296976	4776982	73	216
PO-KD-032	297041	4777025	80	230
PO-KD-033	297121	4777271	85	245
PO-KD-034	297248	4777261	65	238
PO-KD-035	297297	4777354	72	245
PO-KD-036	297494	4777430	65	248
PO-KD-038	297812	4778611	82	80
PO-KD-039	297818	4778591	89	96
PO-KD-040	297729	4778299	84	80
PO-KD-041	297747	4778096	70	261
PO-KD-042	297598	4777898	89	66
PO-KD-043	297308	4777024	60	275

PO-KD-044	297233	4776896	90	28
PO-KD-045	297146	4776587	85	2
PO-KD-046	296873	4776455	65	5
PO-KD-047	296810	4776455	80	30
PO-KD-048	296847	4776406	72	26
PO-KD-050	296716	4776200	90	30
PO-KD-051	296672	4776092	88	27
PO-KD-052	296537	4775692	80	13
PO-KD-053	296416	4775435	69	210
PO-KD-054	307669	4771521	60	225
PO-KD-055	307562	4771817	35	230
PO-KD-056	307431	4772118	30	250
PO-KD-057	307533	4772586	49	260
PO-KD-058	307856	4773126	49	351
PO-KD-060	308094	4773566	52	11
PO-KD-061	308153	4773721	51	350
PO-KD-062	308571	4773919	72	340
PO-KD-063	308622	4774061	70	353
PO-KD-064	308580	4774243	68	360
PO-KD-065	308686	4774359	56	346
PO-KD-066	308726	4774462	56	338
PO-KD-067	309015	4774698	70	336
PO-KD-068	308938	4774799	55	350
PO-KD-069	308401	4775194	35	310
PO-KD-069	308401	4775194	36	330
PO-KD-069	308401	4775194	36	308
PO-KD-069	308401	4775194	43	267
PO-KD-069	308401	4775194	51	252
PO-KD-070	308292	4775079	64	340
PO-KD-071	308384	4775079	32	319
PO-KD-071	308384	4775079	35	314
PO-KD-071	308384	4775079	42	312
PO-KD-072	308388	4775298	32	288
PO-KD-072	308388	4775298	28	294
PO-KD-072	308388	4775298	26	291
PO-KD-073	308388	4775411	42	216
PO-KD-074	308391	4775507	43	213
PO-KD-075	308394	4775343	22	254
PO-KD-076	308394	4775354	32	228
PO-KD-077	308396	4775362	45	245
PO-KD-078	308489	4775357	28	241
PO-KD-079	308830	4775428	40	315
PO-KD-080	308914	4775435	55	220
PO-KD-081	309075	4775456	46	218
PO-KD-082	309037	4775176	36	313
PO-KD-083	309188	4775072	40	336
PO-KD-084	309322	4775055	58	321
PO-KD-085	309359	4774845	62	331
PO-KD-086	309268	4774709	52	325

PO-KD-087	308821	4774295	66	297
PO-KD-088	308659	4774161	77	345
PO-KD-089	298448	4775565	83	205
PO-KD-090	298581	4776049	85	240
PO-KD-091	298792	4776049	60	214
PO-KD-092	298783	4776245	53	236
PO-KD-093	298708	4776409	30	242
PO-KD-094	298611	4776501	38	186
PO-KD-095	298514	4776811	64	210
PO-KD-096	298781	4776754	60	212
PO-KD-097	298938	4776763	65	212
PO-KD-098	299065	4776872	65	224
PO-KD-099	299104	4777044	83	190
PO-KD-100	299084	4777578	60	222
PO-KD-101	299170	4777488	65	204
PO-KD-101	299170	4777488	72	218
PO-KD-102	299470	4777534	71	208
PO-KD-103	299519	4777748	69	211
PO-KD-104	299781	4776613	55	212
PO-KD-105	299909	4776520	70	226
PO-KD-106	299945	4776407	67	216
PO-KD-107	299884	4776035	48	202
PO-KD-108	299939	4775920	53	200
PO-KD-109	299756	4775884	70	206
PO-KD-110	298966	4775903	72	219
PO-KD-111	297775	4776863	90	220
PO-KD-112	297661	4776641	28	268
PO-KD-113	297694	4776577	52	33
PO-KD-114	297823	4776431	64	230
PO-KD-115	297957	4776142	75	205
PO-KD-116	298094	4775838	40	210
PO-KD-117	298371	4776016	38	145
PO-KD-118	298592	4775938	35	220
PO-KD-118	298592	4775938	60	199
PO-KD-119	298605	4774077	80	328
PO-KD-120	298039	4774147	50	120
PO-KD-121	299055	4774160	90	232
PO-KD-122	299215	4774259	60	306
PO-KD-123	299507	4774399	70	288
PO-KD-123	299507	4774399	62	276
PO-KD-124	299685	4774485	83	226
PO-KD-124	299685	4774485	78	224
PO-KD-125	300276	4774584	84	30
PO-KD-125	300276	4774584	79	154
PO-KD-125	300276	4774584	85	174
PO-KD-126	300446	4774970	80	188
PO-KD-127	300853	4775536	65	208
PO-KD-128	300623	4775634	65	203
PO-KD-129	300628	4775726	74	204

PO-KD-130	300725	4775784	88	209
PO-KD-131	300749	4775852	89	208
PO-KD-132	300780	4775903	76	210
PO-KD-133	300848	4776076	76	205
PO-KD-134	299783	4772451	84	238
PO-KD-135	299757	4772357	50	162
PO-KD-136	299719	4772301	67	178
PO-KD-137	299642	4772187	30	156
PO-KD-137	299642	4772187	58	154
PO-KD-138	299351	4771953	30	270
PO-KD-138	299351	4771953	31	264
PO-KD-139	299325	4771805	85	30
PO-KD-139	299325	4771805	58	346
PO-KD-140	299304	4771784	90	255
PO-KD-141	299766	4770268	70	216
PO-KD-142	299751	4770250	53	280
PO-KD-143	299741	4770234	80	31
PO-KD-144	299732	4770245	80	40
PO-KD-145	299720	4770235	80	30
PO-KD-145	299720	4770235	90	30
PO-KD-146	300008	4770304	70	68
PO-KD-147	300077	4770311	88	193
PO-KD-148	300127	4770342	84	343
PO-KD-149	300136	4770409	70	200
PO-KD-149	300136	4770409	70	180
PO-KD-150	300166	4770533	69	195
PO-KD-151	300164	4770558	34	52
PO-KD-152	300135	4770662	82	40
PO-KD-153	300284	4770835	10	328
PO-KD-155	300861	4771385	85	179
PO-KD-156	300983	4771444	54	151
PO-KD-158	308027	4770922	74	347
PO-KD-158	308027	4770922	72	358
PO-KD-158	308027	4770922	73	344
PO-KD-158	308027	4770922	80	4
PO-KD-158	308027	4770922	85	172
PO-KD-158	308027	4770922	85	184
PO-KD-158	308027	4770922	87	184
PO-KD-160	306308	4770750	84	163
PO-KD-160	306308	4770750	72	162
PO-KD-162	305349	4770964	83	192
PO-KD-162	305349	4770964	88	139
PO-KD-163	304858	4771169	66	341
PO-KD-164	304619	4771146	59	338
PO-KD-164	304619	4771146	77	346
PO-KD-164	304619	4771146	40	304
PO-KD-164	304619	4771146	51	314
PO-KD-164	304619	4771146	64	310
PO-KD-164	304619	4771146	88	157

PO-KD-165	303723	4771027	84	205
PO-KD-166	302224	4771281	60	26
PO-KD-167	302158	4771299	70	14
PO-KD-168	302058	4771360	88	318
PO-KD-168	302058	4771360	84	166
PO-KD-169	301914	4771726	35	180
PO-KD-169	301914	4771726	44	181
PO-KD-169	301914	4771726	30	205
PO-KD-170	301922	4771755	45	199
PO-KD-171	302016	4771933	41	171
PO-KD-172	302034	4771997	40	198
PO-KD-173	302157	4772119	40	176
PO-KD-174	302200	4772298	38	196
PO-KD-175	302209	4772331	50	184
PO-KD-175	302209	4772331	40	182
PO-KD-176	302055	4772849	55	188
PO-KD-176	302055	4772849	48	191
PO-KD-177	302044	4772967	65	172
PO-KD-177	302044	4772967	58	186
PO-KD-177	302044	4772967	50	206
PO-KD-177	302044	4772967	44	186
PO-KD-178	302103	4773093	57	222
PO-KD-179	301992	4773004	73	200
PO-KD-180	301962	4773077	46	160
PO-KD-180	301962	4773077	26	191
PO-KD-181	300322	4772942	68	178
PO-KD-181	300322	4772942	75	176
PO-KD-182	298920	4773582	50	180
PO-KD-182	298920	4773582	60	177
PO-KD-182	298920	4773582	63	172
PO-KD-182	298920	4773582	60	174
PO-KD-182	298920	4773582	62	171
PO-KD-183	298610	4774067	75	192
PO-KD-184	298486	4774264	70	318
PO-KD-184	298486	4774264	65	312
PO-KD-184	298486	4774264	77	168
PO-KD-185	298410	4774255	60	340
PO-KD-186	298312	4774376	85	298
PO-KD-187	304518	4771942	88	333
PO-KD-187	304518	4771942	76	336
PO-KD-188	304534	4771924	85	152
PO-KD-189	304474	4772100	64	308
PO-KD-190	304210	4772009	81	324
PO-KD-191	303591	4772148	65	196
PO-KD-192	303567	4772254	66	209
PO-KD-193	303765	4772345	55	214
PO-KD-194	303927	4772330	60	187
PO-KD-194	303927	4772330	65	191
PO-KD-195	303962	4772332	60	182

PO-KD-196	304032	4772347	60	180
PO-KD-197	304113	4772354	55	186
PO-KD-198	304212	4772394	62	166
PO-KD-199	304280	4772397	65	160
PO-KD-200	304562	4772569	90	154
PO-KD-201	304684	4772538	78	328
PO-KD-202	304904	4772480	81	333
PO-KD-203	304923	4772410	60	310
PO-KD-204	305021	4772217	68	333
PO-KD-205	304908	4772190	73	333
PO-KD-206	304670	4771958	75	336
PO-KD-207	304500	4771539	80	150
PO-KD-208	304381	4771454	48	318
PO-KD-209	299057	4772937	70	268
PO-KD-210	299041	4772986	85	99
PO-KD-211	298830	4773019	60	176
PO-KD-212	298784	4772977	74	182
PO-KD-213	298654	4772951	83	346
PO-KD-214	298139	4772724	65	332
PO-KD-215	298066	4772695	90	190
PO-KD-215	298066	4772695	67	230
PO-KD-216	298497	4772887	82	342
PO-KD-217	297779	4776875	90	38
PO-KD-218	297695	4776819	59	135
PO-KD-219	297657	4776719	46	154
PO-KD-220	297670	4776630	59	133
PO-KD-221	297667	4776617	82	158
PO-KD-222	297702	4776577	55	37
PO-KD-222	297702	4776577	54	22
PO-KD-223	297833	4776423	71	228
PO-KD-224	297925	4776245	77	211
PO-KD-224	297925	4776245	34	79
PO-KD-225	297970	4776097	75	202
PO-KD-226	297988	4776015	45	187
PO-KD-227	298093	4775852	53	215
PO-KD-228	298203	4775765	70	165
PO-KD-229	298282	4775990	79	236
PO-KD-230	298374	4776012	69	61
PO-KD-230	298374	4776012	54	68
PO-KD-231	298593	4775939	18	352
PO-KD-232	298650	4775961	54	5
PO-KD-232	298650	4775961	85	199
PO-KD-233	298845	4776015	55	201
PO-KD-233	298845	4776015	55	222
PO-KD-234	298816	4775977	54	252
PO-KD-235	298815	4775725	70	222
PO-KD-236	298923	4775856	74	192
PO-KD-236	298923	4775856	87	196
PO-KD-237	298577	4775550	25	252

PO-KD-237	298577	4775550	26	299
PO-KD-237	298577	4775550	60	249
PO-KD-238	298393	4775382	64	212
PO-KD-238	298393	4775382	50	219
PO-KD-239	298310	4775259	60	198
PO-KD-240	298186	4775263	80	223
PO-KD-241	298139	4775234	86	52
PO-KD-242	298036	4775210	36	196
PO-KD-243	298010	4775188	86	68
PO-KD-244	297932	4775107	84	220
PO-KD-245	298036	4775210	83	32
PO-KD-246	297695	4775015	90	264
PO-KD-247	297483	4775071	69	252
PO-KD-247	297483	4775071	57	270
PO-KD-248	297334	4775171	76	242
PO-KD-249	297371	4775118	59	268
PO-KD-250	297214	4775139	80	243
PO-KD-251	296409	4775376	65	75
PO-KD-252	298616	4774075	90	154
PO-KD-253	298930	4772920	89	141
PO-KD-254	298828	4774162	75	325
PO-KD-255	298882	4774190	70	149
PO-KD-256	298889	4774229	74	166
PO-KD-257	298826	4774265	64	330
PO-KD-257	298826	4774265	80	327
PO-KD-258	298877	4774336	44	302
PO-KD-259	298884	4774344	45	289
PO-KD-260	298903	4774361	43	298
PO-KD-261	298954	4774375	35	313
PO-KD-262	299136	4774289	50	309
PO-KD-263	298540	4774099	83	339
PO-KD-264	298242	4773779	86	139
PO-KD-265	298202	4773761	88	145
PO-KD-266	298138	4773743	80	140
PO-KD-267	298062	4773668	87	323
PO-KD-268	298000	4773616	85	137
PO-KD-269	297942	4773529	81	150
PO-KD-270	297858	4773499	85	151
PO-KD-271	297747	4773396	90	142
PO-KD-272	297770	4773305	80	329
PO-KD-273	297630	4773246	70	155
PO-KD-274	297617	4773380	84	149
PO-KD-275	297617	4773301	64	176
PO-KD-276	297439	4773183	36	225
PO-KD-277	297352	4773073	66	91
PO-KD-277	297352	4773073	16	333
PO-KD-278	297192	4773147	64	352
PO-KD-279	297196	4773256	82	149
PO-KD-280	297059	4773230	51	229

PO-KD-281	294060	4779916	41	355
PO-KD-282	294152	4779961	56	46
PO-KD-283	294255	4780073	70	163
PO-KD-284	294455	4780067	65	208
PO-KD-285	294523	4780066	71	46
PO-KD-286	294347	4780159	75	132
PO-KD-286	294347	4780159	84	136
PO-KD-286	294347	4780159	60	22
PO-KD-286	294347	4780159	54	22
PO-KD-287	293496	4779651	51	351
PO-KD-288	293195	4779327	75	164
PO-KD-289	293158	4779427	87	337
PO-KD-290	293037	4779584	46	333
PO-KD-291	292966	4779707	55	325
PO-KD-292	293727	4780112	86	351
PO-KD-292	293727	4780112	65	167
PO-KD-293	293975	4780277	55	162
PO-KD-294	295134	4780073	76	17
PO-KD-294	295134	4780073	76	5
PO-KD-295	295314	4779858	66	38
PO-KD-297	295730	4779801	66	38
PO-KD-298	295662	4778813	84	21
PO-KD-299	295589	4779849	70	214
PO-KD-300	295509	4779918	85	213
PO-KD-301	295452	4779948	86	34
PO-KD-302	295429	4779977	79	216
PO-KD-303	295381	4780022	80	221
PO-KD-304	294524	4780412	50	39
PO-KD-305	294434	4780527	70	71
PO-KD-305	294434	4780527	75	325
PO-KD-306	294451	4780534	71	33
PO-KD-307	294502	4780689	80	27
PO-KD-308	295639	4780684	63	345
PO-KD-309	294531	4780732	80	35
PO-KD-310	293124	4779585	40	326
PO-KD-311	292212	4778284	24	249
PO-KD-312	303613	4780176	51	198
PO-KD-313	303736	4779791	49	48
PO-KD-314	303804	4779592	35	245
PO-KD-315	303770	4779314	44	126
PO-KD-316	303849	4778838	90	305
PO-KD-317	303789	4778624	68	197
PO-KD-318	303574	4778349	48	328
PO-KD-319	303449	4778245	44	195
PO-KD-320	303363	4778093	55	192
PO-KD-321	303252	4778028	65	230
PO-KD-322	303182	4777892	50	225
PO-KD-323	303099	4777546	55	202
PO-KD-324	303088	4777926	55	218

PO-KD-325	303028	4778078	55	190
PO-KD-326	303022	4778131	60	199
PO-KD-327	302865	4778147	84	195
PO-KD-328	301385	4778361	69	199
PO-KD-329	301246	4778613	75	216
PO-KD-330	301278	4778736	61	201
PO-KD-331	301156	4778652	64	203
PO-KD-332	300875	4778644	61	219
PO-KD-333	300802	4778696	65	226
PO-KD-334	300890	4779470	69	288
PO-KD-335	300892	4779671	46	292
PO-KD-336	301187	4779895	68	323
PO-KD-337	301274	4779944	56	282
PO-KD-338	301448	4780053	45	297
PO-KD-339	301840	4780336	20	187
PO-KD-340	302109	4780347	43	230
PO-KD-341	302741	4780308	79	197
PO-KD-342	303147	4780357	61	18
PO-KD-343	303224	4780504	81	213
PO-KD-344	297821	4789581	48	321
PO-KD-344	297821	4789581	58	320
PO-KD-344	297821	4789581	86	303
PO-KD-345	297963	4789538	62	20
PO-KD-346	298075	4789599	68	292
PO-KD-347	298222	4789648	62	286
PO-KD-348	298823	4789693	85	289
PO-KD-348	298823	4789693	85	286
PO-KD-349	299618	4788908	38	75
PO-KD-349	299618	4788908	9	21
PO-KD-350	299929	4789009	78	289
PO-KD-351	300111	4788918	21	103
PO-KD-352	300544	4788066	30	251
PO-KD-353	301256	4788256	35	274
PO-KD-354	301294	4788768	59	211
PO-KD-355	301343	4788874	34	263
PO-KD-356	301498	4788910	65	202
PO-KD-357	301665	4788956	48	219
PO-KD-358	301751	4788929	41	236
PO-KD-359	302200	4788691	40	254
PO-KD-360	302945	4788212	30	244
PO-KD-361	303765	4787353	36	288
PO-KD-362	304197	4786707	67	256
PO-KD-363	305188	4786346	45	289
PO-KD-364	307088	4784775	71	313
PO-KD-365	306423	4784970	59	303
PO-KD-366	306296	4785810	42	329
PO-KD-367	305920	4786108	28	261
PO-KD-368	303032	4777248	64	209
PO-KD-369	303266	4776884	51	219

PO-KD-370	303356	4776662	62	216
PO-KD-371	303805	4776093	55	217
PO-KD-372	304877	4775394	39	218
PO-KD-373	306546	4775250	62	175
PO-KD-374	307294	4774667	75	238
PO-KD-374	307294	4774667	73	256
PO-KD-375	307898	4775174	71	349
PO-KD-376	309010	4775635	45	215
PO-KD-377	307785	4776573	79	187
PO-KD-378	307462	4776989	34	204
PO-KD-379	307251	4777506	55	198
PO-KD-380	307179	4777878	44	215
PO-KD-382	294291	4786295	34	211
PO-KD-383	294360	4786597	66	226
PO-KD-384	294360	4786597	81	328
PO-KD-385	294223	4787008	81	339
PO-KD-386	294125	4787239	50	327
PO-KD-387	293978	4787731	49	312
PO-KD-388	294001	4787892	35	306
PO-KD-389	293430	4786214	61	175
PO-KD-390	293506	4786407	31	320
PO-KD-391	293615	4786468	85	157
PO-KD-392	293280	4786724	56	32
PO-KD-393	292993	4786998	67	182
PO-KD-394	292977	4787330	44	222
PO-KD-395	292396	4787641	66	6
PO-KD-396	292138	4787077	34	141
PO-KD-397	291722	4787555	79	133
PO-KD-403	302217	4772163	50	193
PO-KD-403	302217	4772163	49	196
PO-KD-404	302200	4772293	42	190
PO-KD-405	302200	4772390	49	197
PO-KD-406	302168	4772560	51	193
PO-KD-406	302168	4772560	60	201
PO-KD-407	302063	4772819	54	205
PO-KD-408	302044	4772970	60	180
PO-KD-408	302044	4772970	54	182
PO-KD-410	297699	4776580	51	34
PO-KD-411	297822	4776425	66	234
PO-KD-412	297914	4776248	82	217
PO-KD-414	298604	4775937	50	18
PO-KD-420	298393	4775391	79	209
PO-KD-421	298310	4775259	76	216
PO-KD-421	298310	4775259	66	207
PO-KD-422	298185	4775255	87	213
PO-KD-427	297449	4775075	42	236
PO-KD-427	297449	4775075	36	254
PO-KD-427	297449	4775075	42	249
PO-KD-430	302146	4772146	5	278

PO-KD-431	302080	4772788	54	184
PO-KD-432	302050	4772843	54	184
PO-KD-433	302925	4788250	30	255
PO-KD-434	302767	4788431	31	254
PO-KD-434	302767	4788431	31	224
PO-KD-436	302738	4788516	30	256
PO-KD-437	302738	4788516	25	246
PO-KD-438	293832	4785477	59	309
PO-KD-438	293932	4785477	52	317
PO-KD-438	293932	4785477	82	297
PO-KD-438	293932	4785477	84	152
PO-KD-438	293932	4785477	81	152
PO-KD-438	293932	4785477	88	154
PO-KD-439	293954	4784806	67	141
PO-KD-439	293954	4784806	77	142
PO-KD-439	293954	4784806	73	150
PO-KD-439	293954	4784806	86	312
PO-KD-440	293949	4784692	60	176
PO-KD-440	293949	4784692	56	197
PO-KD-440	293949	4784692	56	213
PO-KD-441	293836	4784554	57	181
PO-KD-441	293836	4784554	57	177
PO-KD-441	293836	4784554	61	167
PO-KD-441	293836	4784554	72	167
PO-KD-442	293908	4784425	72	160
PO-KD-442	293908	4784425	74	162
PO-KD-443	294110	4784206	53	157
PO-KD-443	294110	4784206	50	170
PO-KD-444	293205	4784098	79	175
PO-KD-445	294168	4783990	70	148
PO-KD-445	294168	4783990	35	235
PO-KD-446	294285	4784064	56	169
PO-KD-446	294285	4784064	58	190
PO-KD-447	294288	4783983	71	151
PO-KD-448	294283	4783958	73	105
PO-KD-448	294283	4783958	75	108
PO-KD-448	294283	4783958	78	310
PO-KD-448	294283	4783958	69	307
PO-KD-449	294352	4783882	85	150
PO-KD-449	294352	4783882	86	143
PO-KD-449	294352	4783882	79	155
PO-KD-449	294352	4783882	83	147
PO-KD-450	294439	4783770	74	148
PO-KD-450	294439	4783770	77	140
PO-KD-451	294300	4783667	72	149
PO-KD-451	294300	4783667	71	156
PO-KD-452	294349	4783558	83	152
PO-KD-452	294349	4783558	81	142
PO-KD-453	294388	4783400	72	138

PO-KD-454	294440	4783251	75	350
PO-KD-454	294440	4783251	72	346
PO-KD-456	294474	4783177	80	6
PO-KD-456	294474	4783177	85	359
PO-KD-457	294562	4783186	83	347
PO-KD-457	294562	4783186	90	180
PO-KD-458	294562	4783337	87	166
PO-KD-459	294621	4783251	75	335
PO-KD-459	294621	4783251	78	323
PO-KD-459	294621	4783251	55	320
PO-KD-459	294621	4783251	47	323
PO-KD-461	294761	4783127	61	157
PO-KD-462	294881	4783235	65	320
PO-KD-462	294881	4783235	76	327
PO-KD-463	294833	4783354	48	192
PO-KD-463	294833	4783354	76	182
PO-KD-463	294833	4783354	79	172
PO-KD-465	293942	4783385	76	323
PO-KD-465	293942	4783385	59	155
PO-KD-465	293942	4783385	70	347
PO-KD-466	295027	4783257	80	327
PO-KD-467	295086	4782919	56	186
PO-KD-467	295086	4782919	61	179
PO-KD-467	295086	4782919	57	170
PO-KD-468	295096	4782725	80	182
PO-KD-468	295096	4782725	90	357
PO-KD-468	295096	4782725	84	186
PO-KD-470	299129	4785924	46	301
PO-KD-471	298922	4785421	65	163
PO-KD-471	298922	4785421	72	175
PO-KD-473	298947	4785029	77	340
PO-KD-473	298947	4785029	75	355
PO-KD-473	298947	4785029	83	5
PO-KD-473	298947	4785029	83	355
PO-KD-474	298960	4784824	84	164
PO-KD-474	298960	4784824	86	172
PO-KD-474	298960	4784824	83	172
PO-KD-475	298961	4784731	81	179
PO-KD-475	298961	4784731	83	179
PO-KD-475	298961	4784731	80	179
PO-KD-475	298961	4784731	86	173
PO-KD-476	299130	4784711	87	179
PO-KD-476	299130	4784711	84	357
PO-KD-476	299130	4784711	88	3
PO-KD-477	299170	4784642	77	351
PO-KD-477	299170	4784642	78	346
PO-KD-478	299232	4784463	78	179
PO-KD-478	299232	4784463	72	193
PO-KD-478	299232	4784463	81	183

PO-KD-479	299107	4784333	85	168
PO-KD-479	299107	4784333	85	176
PO-KD-480	299041	4784237	82	176
PO-KD-481	298953	4784148	84	354
PO-KD-481	298953	4784148	86	353
PO-KD-481	298953	4784148	78	357
PO-KD-482	298673	4784009	90	353
PO-KD-482	298673	4784009	89	353
PO-KD-483	298631	4783886	79	11
PO-KD-483	298631	4783886	81	353
PO-KD-484	298716	4783708	72	162
PO-KD-484	298716	4783708	83	181
PO-KD-485	298784	4783680	72	163
PO-KD-485	298784	4783680	75	174
PO-KD-486	298763	4783503	88	354
PO-KD-486	298763	4783503	87	354
PO-KD-487	298766	4783398	71	172
PO-KD-487	298766	4783398	77	177
PO-KD-487	298766	4783398	81	179
PO-KD-487	298766	4783398	77	179
PO-KD-488	298819	4783107	72	2
PO-KD-488	298819	4783107	74	359
PO-KD-488	298819	4783107	71	16
PO-KD-489	298811	4782788	70	177
PO-KD-489	298811	4782788	68	162
PO-KD-489	298811	4782788	79	182
PO-KD-490	298746	4782642	79	172
PO-KD-492	298679	4782505	62	207
PO-KD-492	298679	4782505	54	211
PO-KD-492	298679	4782505	62	210
PO-KD-493	298658	4782409	72	204
PO-KD-493	298658	4782409	77	212
PO-KD-493	298658	4782409	78	211
PO-KD-494	298700	4782248	69	192
PO-KD-494	298700	4782248	78	207
PO-KD-494	298700	4782248	77	184
PO-KD-494	298700	4782248	81	195
PO-KD-495	298719	4782163	68	195
PO-KD-495	298789	4782163	80	193
PO-KD-495	298789	4782163	72	198
PO-KD-496	298789	4781985	74	189
PO-KD-496	298789	4781985	84	187
PO-KD-497	298741	4781787	62	187
PO-KD-497	298741	4781787	74	202
PO-KD-497	298741	4781787	65	203
PO-KD-497	298741	4781787	71	203
PO-KD-497	298741	4781787	72	191
PO-KD-497	298741	4781787	74	210
PO-KD-498	298693	4781666	78	199

PO-KD-498	298693	4781666	80	193
PO-KD-498	298693	4781666	72	196
PO-KD-499	298655	4781578	71	198
PO-KD-499	298655	4781578	79	189
PO-KD-500	298512	4781516	75	195
PO-KD-500	298512	4781516	84	190
PO-KD-501	298410	4781435	80	196
PO-KD-501	298410	4781435	76	202
PO-KD-502	298276	4781406	70	200
PO-KD-502	298276	4781406	58	201
PO-KD-502	298276	4781406	76	191
PO-KD-503	298192	4781303	79	201
PO-KD-504	298176	4781234	71	180
PO-KD-504	298176	4781234	72	186
PO-KD-505	298117	4781216	87	3
PO-KD-505	298117	4781216	89	193
PO-KD-505	298117	4781216	90	9
PO-KD-505	298117	4781216	87	189
PO-KD-505	298117	4781216	86	186
PO-KD-506	298013	4781118	75	191
PO-KD-506	298013	4781118	79	195
PO-KD-506	298013	4781118	83	197
PO-KD-506	298013	4781118	80	189
PO-KD-508	297829	4781050	74	20
PO-KD-508	297829	4781050	77	11
PO-KD-508	297829	4781050	75	14
PO-KD-509	297841	4780953	89	13
PO-KD-509	297841	4780953	86	194
PO-KD-509	297841	4780953	85	8
PO-KD-510	297617	4780709	89	4
PO-KD-510	297617	4780709	79	3
PO-KD-510	297617	4780709	77	1
PO-KD-511	297454	4780255	86	206
PO-KD-511	297454	4780255	84	215
PO-KD-512	297502	4780087	72	210
PO-KD-513	297524	4780086	78	343
PO-KD-515	297605	4780009	74	72
PO-KD-515	297605	4780009	76	74
PO-KD-515	297605	4780009	72	76
PO-KD-516	300383	4785898	31	247
PO-KD-516	300383	4785898	34	260
PO-KD-516	300383	4785898	52	250
PO-KD-516	300383	4785898	44	257
PO-KD-517	300425	4784842	73	17
PO-KD-517	300425	4784842	81	183
PO-KD-518	300425	4784842	81	3
PO-KD-518	300425	4784842	82	359
PO-KD-518	300425	4784842	85	351
PO-KD-518	300425	4784842	79	355

PO-KD-519	300593	4784581	85	357
PO-KD-520	300567	4784478	85	172
PO-KD-520	300567	4784478	84	163
PO-KD-520	300567	4784478	89	175
PO-KD-521	300648	4784356	82	360
PO-KD-521	300648	4784356	84	353
PO-KD-521	300648	4784356	78	347
PO-KD-522	300739	4784082	90	171
PO-KD-522	300739	4784082	84	358
PO-KD-522	300739	4784082	84	349
PO-KD-522	300739	4784082	83	346
PO-KD-523	300857	4783986	80	183
PO-KD-523	300857	4783986	78	167
PO-KD-523	300857	4783986	72	185
PO-KD-524	300930	4783714	68	194
PO-KD-524	300930	4783714	70	188
PO-KD-524	300930	4783714	71	188
PO-KD-525	300911	4783630	79	190
PO-KD-525	300911	4783630	77	176
PO-KD-525	300911	4783630	79	176
PO-KD-525	300911	4783630	78	177
PO-KD-526	301092	4783629	58	173
PO-KD-526	301092	4783629	62	172
PO-KD-526	301092	4783629	59	173
PO-KD-527	301172	4783648	64	172
PO-KD-527	301172	4783648	58	358
PO-KD-528	301443	4783606	69	345
PO-KD-528	301443	4783606	72	348
PO-KD-528	301443	4783606	65	346
PO-KD-529	301604	4783520	45	357
PO-KD-529	301604	4783520	44	357
PO-KD-529	301604	4783520	45	358
PO-KD-529	301604	4783520	83	359
PO-KD-529	301604	4783520	85	2
PO-KD-529	301604	4783520	86	3
PO-KD-529	301604	4783520	83	359
PO-KD-530	301631	4783390	61	4
PO-KD-530	301631	4783390	64	7
PO-KD-530	301631	4783390	53	14
PO-KD-531	301496	4783807	37	336
PO-KD-531	301496	4783807	45	335
PO-KD-531	301496	4783807	48	337
PO-KD-532	302215	4783679	54	196
PO-KD-532	302215	4783679	71	205
PO-KD-532	302215	4783679	62	301
PO-KD-532	302215	4783679	62	185
PO-KD-533	302248	4783534	72	181
PO-KD-533	302248	4783534	60	188
PO-KD-533	302248	4783534	66	189

PO-KD-533	302248	4783534	70	184
PO-KD-534	302138	4783883	66	347
PO-KD-534	302138	4783883	72	345
PO-KD-534	302138	4783883	57	340
PO-KD-535	302071	4783981	87	351
PO-KD-535	302071	4783981	89	357
PO-KD-535	302071	4783981	88	359
PO-KD-536	302197	4784217	76	3
PO-KD-536	302197	4784217	88	184
PO-KD-536	302197	4784217	85	184
PO-KD-536	302197	4784217	84	175
PO-KD-537	302217	4784333	75	12
PO-KD-537	302217	4784333	80	360
PO-KD-537	302217	4784333	74	6
PO-KD-537	302217	4784333	70	356
PO-KD-539	302228	4784533	64	321
PO-KD-539	302228	4784533	61	327
PO-KD-539	302228	4784533	60	344
PO-KD-539	302228	4784533	72	349
PO-KD-539	302228	4784533	73	348
PO-KD-539	302228	4784533	65	353
PO-KD-540	302393	4784513	89	27
PO-KD-540	302393	4784513	88	18
PO-KD-540	302393	4784513	80	18
PO-KD-540	302393	4784513	82	19
PO-KD-540	302393	4784513	66	352
PO-KD-540	302393	4784513	69	347
PO-KD-540	302393	4784513	65	347
PO-KD-540	302393	4784513	62	337
PO-KD-541	302745	4784519	77	346
PO-KD-541	302745	4784519	79	347
PO-KD-541	302745	4784519	69	344
PO-KD-542	302820	4784687	70	348
PO-KD-542	302820	4784687	65	342
PO-KD-542	302820	4784687	72	342
PO-KD-542	302820	4784687	69	343
PO-KD-543	302839	4784904	53	322
PO-KD-543	302839	4784904	49	331
PO-KD-543	302839	4784904	51	326
PO-KD-544	302911	4785090	62	298
PO-KD-544	302911	4785090	60	300
PO-KD-545	303013	4785155	55	291
PO-KD-545	303013	4785155	55	292
PO-KD-545	303013	4785155	48	295
PO-KD-545	303013	4785155	55	287
PO-KD-546	303066	4785369	72	305
PO-KD-546	303066	4785369	80	302
PO-KD-546	303066	4785369	76	306
PO-KD-547	303006	4785720	50	275

PO-KD-547	303006	4785720	60	287
PO-KD-547	303006	4785720	59	265
PO-KD-551	300531	4785941	44	303
PO-KD-552	298756	4785252	42	34
PO-KD-552	298756	4785252	48	34
PO-KD-552	298756	4785252	32	40
PO-KD-552	298756	4785252	38	36
PO-KD-553	298741	4785334	71	197
PO-KD-553	298741	4785334	71	196
PO-KD-553	298741	4785335	46	276
PO-KD-553	298741	4785335	44	268
PO-KD-553	298741	4785335	45	274
PO-KD-554	298558	4785330	45	346
PO-KD-554	298558	4785330	41	352
PO-KD-554	298558	4785330	45	352
PO-KD-554	298558	4785330	36	346
PO-KD-554	298558	4785330	50	331
PO-KD-555	298520	4785179	42	354
PO-KD-555	298520	4785179	44	347
PO-KD-555	298520	4785179	55	343
PO-KD-556	298444	4785416	51	323
PO-KD-556	298444	4785416	51	322
PO-KD-556	298444	4785416	40	322
PO-KD-556	298444	4785416	39	327
PO-KD-557	298413	4785528	78	318
PO-KD-557	298413	4785528	77	333
PO-KD-557	298413	4785528	84	336
PO-KD-558	298267	4785577	71	323
PO-KD-558	298267	4785577	75	319
PO-KD-558	298267	4785577	79	315
PO-KD-558	298267	4785577	77	320
PO-KD-559	298179	4785661	74	318
PO-KD-559	298179	4785661	70	324
PO-KD-559	298179	4785661	71	320
PO-KD-560	298140	4785781	55	317
PO-KD-560	298140	4785781	54	323
PO-KD-560	298140	4785781	48	319
PO-KD-561	298042	4785725	62	319
PO-KD-561	298042	4785725	67	316
PO-KD-561	298042	4785725	62	317
PO-KD-562	297903	4785829	47	310
PO-KD-563	298132	4786026	59	353
PO-KD-563	298132	4786026	56	344
PO-KD-563	298132	4786026	59	347
PO-KD-565	298158	4786273	25	257
PO-KD-565	298158	4786273	26	263
PO-KD-565	298158	4786273	32	257
PO-KD-566	298260	4786377	71	19
PO-KD-566	298260	4786377	72	347

PO-KD-566	298260	4786377	69	337
PO-KD-566	298260	4786377	68	332
PO-KD-566	298260	4786377	73	326
PO-KD-566	298260	4786377	80	316
PO-KD-567	298242	4786782	39	289
PO-KD-567	298242	4786782	37	297
PO-KD-567	298242	4786782	53	278
PO-KD-567	298242	4786782	44	277
PO-KD-567	298242	4786782	55	274
PO-KD-567	298242	4786782	58	274
PO-KD-568	298249	4787009	77	326
PO-KD-568	298249	4787009	80	326
PO-KD-568	298249	4787009	76	328
PO-KD-568	298249	4787009	74	317
PO-KD-569	298249	4787009	86	287
PO-KD-569	298249	4787009	85	297
PO-KD-569	298249	4787009	86	284
PO-KD-569	298249	4787009	80	285
PO-KD-570	298280	4787317	85	249
PO-KD-570	298280	4787317	76	248
PO-KD-570	298280	4787317	72	244
PO-KD-571	298270	4787450	61	237
PO-KD-571	298270	4787450	54	222
PO-KD-571	298270	4787450	58	242
PO-KD-571	298270	4787450	58	240
PO-KD-572	298262	4787506	78	48
PO-KD-572	298262	4787506	74	52
PO-KD-572	298262	4787506	79	43
PO-KD-573	298729	4787839	81	280
PO-KD-573	298729	4787839	77	274
PO-KD-573	298729	4787839	80	272
PO-KD-573	298729	4787839	76	274
PO-KD-574	298286	4787978	85	343
PO-KD-574	298286	4787978	87	355
PO-KD-574	298286	4787978	87	351
PO-KD-575	298311	4788032	79	327
PO-KD-575	298311	4788032	80	335
PO-KD-575	298311	4788032	76	323
PO-KD-575	298311	4788032	73	331
PO-KD-575	298311	4788032	75	329
PO-KD-575	298311	4788032	81	289
PO-KD-575	298311	4788032	76	268
PO-KD-575	298311	4788032	78	264
PO-KD-576	298374	4788131	48	317
PO-KD-576	298374	4788131	44	343
PO-KD-576	298374	4788131	45	322
PO-KD-576	298374	4788131	43	319
PO-KD-577	298432	4788228	52	283
PO-KD-577	298432	4788228	51	284

PO-KD-577	298432	4788228	54	280
PO-KD-578	298446	4788281	63	267
PO-KD-579	298545	4788626	25	253
PO-KD-579	298545	4788626	26	250
PO-KD-579	298545	4788626	26	252
PO-KD-580	298585	4788675	49	251
PO-KD-580	298585	4788675	67	257
PO-KD-580	298585	4788626	58	255
PO-KD-580	298585	4788626	64	262
PO-KD-581	298595	4788741	73	263
PO-KD-581	298595	4788741	75	263
PO-KD-581	298595	4788741	64	258
PO-KD-582	298683	4788578	68	274
PO-KD-582	298683	4788578	69	272
PO-KD-582	298683	4788578	59	267
PO-KD-583	298764	4788590	68	276
PO-KD-583	298764	4788590	67	272
PO-KD-583	298764	4788590	64	270
PO-KD-583	298764	4788590	71	272
PO-KD-584	298866	4788502	76	286
PO-KD-584	298866	4788502	72	289
PO-KD-584	298866	4788502	73	286
PO-KD-584	298866	4788502	69	282
PO-KD-585	299144	4788564	88	267
PO-KD-585	299144	4788564	86	274
PO-KD-585	299144	4788564	82	266
PO-KD-585	299144	4788564	80	263

Table A - 2 Station, location and orientation of fold axes measurements

Station	Easting	Northing	Dip	Dip Direction
PO-KD-019	303260	4773399	68	18
PO-KD-019	303260	4773399	68	10
PO-KD-019	303260	4773399	68	20
PO-KD-024	296396	4776446	80	330
PO-KD-024	296396	4776446	78	324
PO-KD-028	296457	4776727	72	50
PO-KD-029	296388	4777073	70	290
PO-KD-037	297619	4777616	70	209
PO-KD-049	296822	4776223	40	288
PO-KD-049	296822	4776223	42	287
PO-KD-059	308030	4773291	15	355
PO-KD-064	308580	4774243	38	40
PO-KD-064	308580	4774243	39	345
PO-KD-066	308726	4774462	79	235
PO-KD-066	308726	4774462	39	217
PO-KD-066	308726	4774462	45	212
PO-KD-066	308726	4774462	38	196
PO-KD-068	308938	4774799	30	54
PO-KD-085	309359	4774845	55	40
PO-KD-125	300276	4774584	64	284
PO-KD-125	300276	4774584	62	282
PO-KD-125	300276	4774584	72	268
PO-KD-136	299719	4772301	45	135
PO-KD-136	299719	4772301	50	135
PO-KD-162	305349	4770964	40	260
PO-KD-164	304619	4771146	20	38
PO-KD-164	304619	4771146	0	55
PO-KD-189	304474	4772100	48	248
PO-KD-296	295694	4779772	30	315
PO-KD-400	301882	4771755	46	86
PO-KD-402	302130	4772058	28	3
PO-KD-403	302217	4772163	25	90
PO-KD-411	297822	4776425	36	316
PO-KD-411	297822	4776425	43	156
PO-KD-413	297966	4776090	23	260
PO-KD-416	298800	4775932	44	144
PO-KD-417	298814	4775830	38	264
PO-KD-418	298578	4775552	34	314
PO-KD-419	298419	4775430	27	108
PO-KD-419	298419	4775430	31	110
PO-KD-426	297672	4775030	7	144
PO-KD-448	294283	4783958	20	303
PO-KD-564	298150	4786133	30	330
PO-KD-566	298260	4786377	75	355
PO-KD-575	298311	4788032	80	315